AMERICAN SOCIETY FOR MICROBIOLOGY | Journal of Virology®

VIRUS-CELL INTERACTIONS

Human Immunodeficiency Virus Type 1 Vpr Mediates Degradation of APC1, a Scaffolding Component of the Anaphase-Promoting Complex/Cyclosome

Jérémy A. Ferreira Barbosa,[a] Samantha Sparapani,[a] Jonathan Boulais,[a] Robert Lodge,[a] Éric A. Cohen[a,b]

[a]Montreal Clinical Research Institute, Montréal, Québec, Canada
[b]Department of Microbiology, Infectiology and Immunology, Université de Montréal, Montréal, Québec, Canada

ABSTRACT HIV-1 encodes several accessory proteins—Nef, Vif, Vpr, and Vpu—whose functions are to modulate the cellular environment to favor immune evasion and viral replication. While Vpr was shown to mediate a G_2/M cell cycle arrest and provide a replicative advantage during infection of myeloid cells, the mechanisms underlying these functions remain unclear. In this study, we defined HIV-1 Vpr proximity interaction network using the BioID proximity labeling approach and identified 352 potential Vpr partners/targets, including several complexes, such as the cell cycle-regulatory anaphase-promoting complex/cyclosome (APC/C). Herein, we demonstrate that both the wild type and cell cycle-defective mutants of Vpr induce the degradation of APC1, an essential APC/C scaffolding protein, and show that this activity relies on the recruitment of DCAF1 by Vpr and the presence of a functional proteasome. Vpr forms a complex with APC1, and the APC/C coactivators Cdh1 and Cdc20 are associated with these complexes. Interestingly, we found that Vpr encoded by the prototypic HIV-1 NL4.3 does not interact efficiently with APC1 and is unable to mediate its degradation as a result of a N28S-G41N amino acid substitution. In contrast, we show that APC1 degradation is a conserved feature of several primary Vpr variants from transmitted/founder virus. Functionally, Vpr-mediated APC1 degradation did not impact the ability of the protein to induce a G_2 cell cycle arrest during infection of $CD4^+$ T cells or enhance HIV-1 replication in macrophages, suggesting that this conserved activity may be important for other aspects of HIV-1 pathogenesis.

IMPORTANCE The function of the Vpr accessory protein during HIV-1 infection remains poorly defined. Several cellular targets of Vpr were previously identified, but their individual degradation does not fully explain the ability of Vpr to impair the cell cycle or promote HIV-1 replication in macrophages. Here, we used the unbiased proximity labeling approach, called BioID, to further define the Vpr proximity interaction network and identified several potentially new Vpr partners/targets. We validated our approach by focusing on a cell cycle master regulator, the APC/C complex, and demonstrated that Vpr mediated the degradation of a critical scaffolding component of APC/C called APC1. Furthermore, we showed that targeting of APC/C by Vpr did not impact the known activity of Vpr. Since degradation of APC1 is a conserved feature of several primary variants of Vpr, it is likely that the interplay between Vpr and APC/C governs other aspects of HIV-1 pathogenesis.

KEYWORDS anaphase-promoting complex/cyclosome, proximity labeling, proteomics, APC1, BioID, HIV infection, human immunodeficiency virus, Vpr, cell cycle regulation

All primate lentiviruses, including human immunodeficiency virus types 1 and 2 (HIV-1/2), encode a set of accessory proteins primarily involved in promoting viral immune evasion and replication (1). Of all the lentivirus-encoded accessory proteins,

Citation Barbosa JAF, Sparapani S, Boulais J, Lodge R, Cohen ÉA. 2021. Human immunodeficiency virus type 1 Vpr mediates degradation of APC1, a scaffolding component of the anaphase-promoting complex/cyclosome. J Virol 95:e00971-20. https://doi.org/10.1128/JVI.00971-20.

Editor Frank Kirchhoff, Ulm University Medical Center

Address correspondence to Éric A. Cohen, Eric.Cohen@ircm.qc.ca.

Received 20 May 2020
Accepted 5 May 2021
Accepted manuscript posted online 19 May 2021
Published 12 July 2021

Viral protein R (Vpr) remains the most enigmatic at the functional level. HIV-1 Vpr is a 14-kDa protein that is packaged into virions, pointing to an early role in the virus life cycle. The protein is required for HIV pathogenesis *in vivo* and for efficient virus replication in macrophages. However, the mechanisms underlying these phenotypes remain elusive (2). One well-established but poorly understood Vpr-associated phenotype is its ability to activate DNA damage response (DDR)/repair pathways, a condition that leads to a G_2/M cell cycle arrest (3, 4). This biological activity requires the recruitment of the E3 ubiquitin ligase complex DDB1-CUL4A-DCAF1 (DCAF1com). However, while the recruitment of DCAF1com is necessary to induce a G_2/M cell cycle arrest, it is not sufficient, as demonstrated by well-characterized G_2/M arrest-defective Vpr mutants that are impaired in (Q65R) or still competent for (S79A or R80A) complex formation with DCAF1com (5–9). Indeed, Vpr recruits DCAF1com to mediate polyubiquitination and subsequent proteasomal degradation of several cellular targets (10), including the DNA repair proteins UNG2, HLTF, EXO1, and MUS81, a component of the SLX4 complex (11–16). Nonetheless, the degradation of these cellular targets by Vpr, at least individually, does not explain the Vpr-mediated activation of the DNA replication/damage checkpoint in G_2/M (11–16).

Recruitment of DCAF1com by Vpr and proteasomal degradation of host cellular proteins appear to contribute to the enhancement of HIV-1 replication in myeloid cells, such as macrophages (17). For example, proteins belonging to the TET family of methylcytosine dioxygenase (TET1/2/3), involved in transcriptional regulation, are reported to be degraded by Vpr in a DCAF1com-dependent manner (18). By mediating TET2 degradation, Vpr affects the transcription of at least two cellular genes encoding the cytokine interleukin 6 (IL-6) and the antiviral restriction factor IFTM3 (18, 19). While sustained IL-6 production by Vpr-mediated TET2 degradation is reported to promote HIV-1 replication in macrophages, decreased expression of IFTM3 enhances HIV-1 infectivity by increasing Env processing and incorporation into virions (18, 19). More recently, the macrophage mannose receptor (MR) was identified as an HIV-1 restriction factor targeting Env in primary macrophages and Vpr, along with Nef, was found to counteract this restriction by reducing MR expression (20). Vpr was also found to induce the degradation of REAF, a protein that inhibits HIV-1 reverse transcription during macrophage infection (21).

Several studies have applied unbiased proteomic approaches to identify novel Vpr host partners/targets. For instance, both Jäger et al. (22) and Hrecka et al. (11) mapped Vpr's interactome through affinity purification coupled to mass spectrometry (AP-MS) and identified 47 high-confidence proteins and HLTF, a new Vpr target, respectively. Using a quantitative proteomics approach, Lahouassa et al. demonstrated that Vpr mediates HLTF degradation (12), whereas Greenwood et al. identified nearly 2,000 cellular proteins modulated directly or indirectly by Vpr (23). Indeed, the demonstration of a promiscuous targeting of cellular proteins by Vpr supports the notion that this viral protein is unlikely to target one unique cellular protein or complex to mediate cell cycle arrest or promote viral replication in myeloid cells. Instead, remodeling of multiple host factors is likely to underpin the complex Vpr-associated phenotypes (11, 24).

Using the Vpr mutants Q65R and R80A, as well as the wild-type (WT) form, we applied BioID, a proximity-dependent labeling biotin-identification approach, to identify stable, weak, or transient Vpr interactions unidentified by previous AP-MS screens (25). Our BioID results define 352 Vpr partners/targets with previously reported Vpr targets or partners, such as UNG (16), EXO1 (13), DCAF1com (5–7), and the SMN complex (22, 23). Interestingly, our analysis also revealed novel potential Vpr partners/targets, including the anaphase-promoting complex/cyclosome (APC/C).

APC/C is a large (1.5-MDa) E3 ubiquitin ligase complex composed of 14 subunits and two coactivators, namely, Cdh1 and Cdc20, that marks target cell cycle proteins for degradation by the proteasome (see reference 26 for a review). While the APC/C^{Cdh1} complex activity peaks during the G_1 phase of the cell cycle, APC/C^{Cdc20} activity peaks in the M phase (27, 28). Besides regulating the cell cycle, APC/C is implicated in

additional processes, including DDR/repair, synthesis of deoxynucleoside triphosphates (dNTPs), autophagy, and cellular metabolism (29). Interestingly, several proteins from both RNA and DNA viruses interact with APC/C to manipulate the host during infection, although in most cases the relevance of these interactions for viral replication remains poorly understood (30).

Given the importance of the APC1 scaffolding subunit (also called ANAPC1) in APC/C architecture and stability, we focused our analysis on the interplay of HIV-1 Vpr and APC1 (31). We show that HIV-1 Vpr forms a physical complex with APC1 and mediates its proteasomal degradation by a process that relies on DCAF1com recruitment. We further demonstrate that Vpr-mediated APC1 degradation is a conserved feature of several primary and lab-adapted Vpr variants but not of the prototypic NL4.3 Vpr, which does not interact efficiently with APC 1. By comparing the Vpr variant Bru, which is competent for APC1 degradation, to NL4.3 Vpr, we delineated N28S and G41N amino acid mutations responsible for the NL4.3 Vpr defect and further demonstrated that APC1 degradation and the induction of a G_2/M cell cycle arrest are two independent activities of Vpr. Last, we show that the replication kinetics of viruses encoding WT Vpr or a Vpr containing the N28S-G41N double substitution in activated primary $CD4^+$ T cells and monocyte-derived macrophages (MDMs) are indistinguishable, thus pointing to APC1 degradation and conceivably APC/C impairment as a new biological activity of Vpr with currently undefined functional implications for HIV-1 pathogenesis.

RESULTS

Analysis of the HIV-1 Vpr proximity interaction network uncovers potential new host partners/targets. To gain insight into Vpr interactions with host cell proteins and processes, we took advantage of the BioID proximity labeling approach (25). This approach relies on the biotinylation of proximal proteins, which can then be pulled down through high-affinity streptavidin-biotin interactions for identification by mass spectrometry. To this end, we fused the highly active *Escherichia coli* biotin ligase ($BirA^{R118G}$, annotated as BirA*) at the N terminus of WT Vpr (Bru) or of G_2/M cell cycle arrest-defective mutants (Q65R and R80A). We reasoned that introduction of Vpr mutants in these analyses would expand the coverage of Vpr partners/targets that would either be degraded in the context of the WT Vpr-DCAF1 complex or be absent from this complex under conditions in which a G_2/M cell cycle arrest was induced. Since Vpr is a nuclear protein, a BirA* fused to a nuclear localization signal (NLS) sequence was used as a negative control to exclude the BirA*-specific proximity interaction network. Doxycycline-inducible HEK293 and HeLa cell lines stably expressing these constructs were generated using the Flp-In T-REx system. BioID screens were then performed in biological duplicates at 6 h and 24 h post-doxycycline induction (hpi) in HEK293 cells as well as at 24 hpi in HeLa cells, as described in Materials and Methods. After performing significance analysis of interactome (SAINT analysis) for each bait and for every time of induction in both cell lines, preys passing the statistical threshold (iProphet protein probability ≥ 0.9; number of unique peptides ≥ 2; Bayesian false discovery rate [BFDR] ≤ 0.02) were kept and merged, constituting the global Vpr proximity interaction network from both HEK293 and HeLa cell lines (Fig. 1A; also, see Table S1 in the supplemental material). A total of 352 proximity interactors were identified in our Vpr proximity interaction network analysis. The analysis was validated by the presence of previously identified Vpr partners/targets, including: DCAF1 (5–7), DDB1 (5–7), UNG (16), EXO1 (13), DICER1 (32), and components of the SMN complex (22, 23). Overrepresented biological processes, such as cell cycle, RNA processing, response to DNA damage, and gene expression, were found among Vpr's preys (Fig. 1A). Interestingly, we identified core elements from several complexes, such as the APC/C (26); the ORC complex, implicated in transcriptional silencing and DNA replication (33); the RISC-loading complex, implicated in RNA silencing mediated by small RNAs (34); the CCR4-NOT complex, involved in transcriptional regulation and RNA surveillance (35); and the SMN complex, involved in the biogenesis of spliceosomal small nuclear ribonucleoproteins (36).

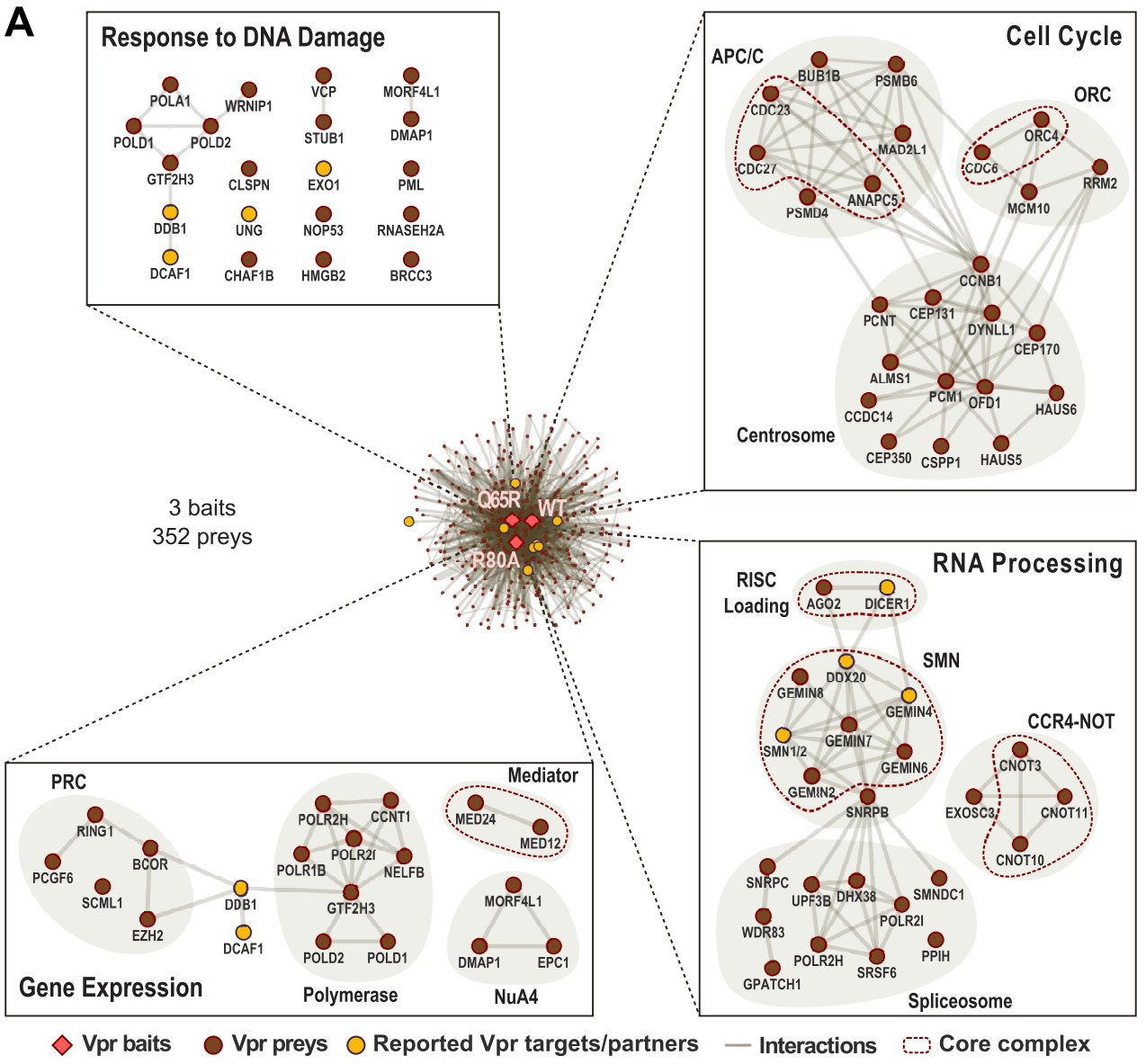

FIG 1 Large-scale HIV-1 Vpr proximity interaction network. HEK293 Flp-In T-REx and HeLa Flp-In T-REx stable cell lines were treated for 6 or 24 h with 0.5 μg/ml doxycycline to induce BirA*-Flag-Vpr (Bru) (WT, Q65R, or R80A) or Flag-NLS-BirA* fusion protein expression. Biotin (50 μM for 6 or 24 h) and MG-132 (10 μM for 6 h) were also added at the same time as doxycycline to allow biotinylation of proximal partners/targets and

(Continued on next page)

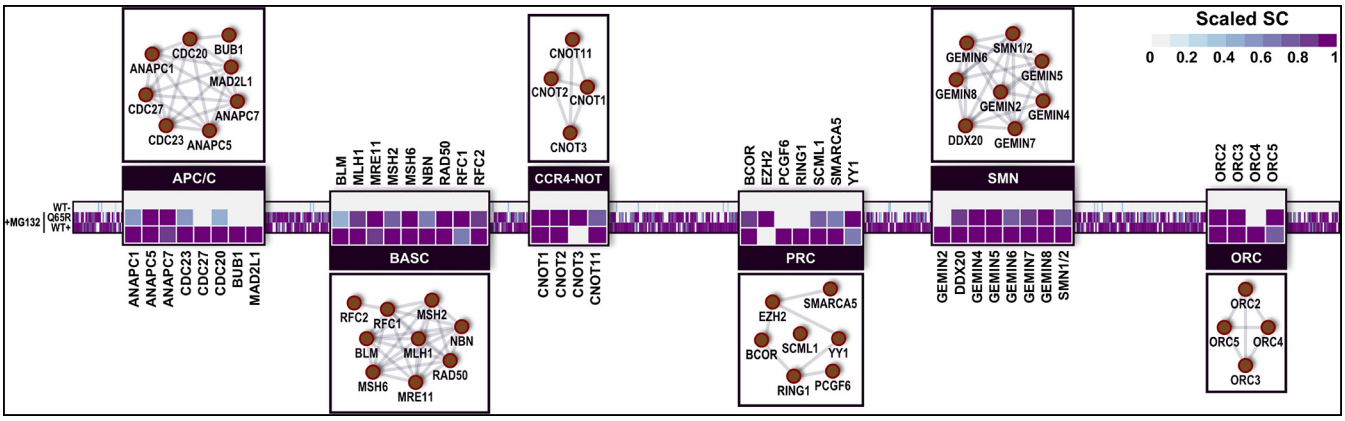

FIG 2 The Vpr proximity interaction network reveals host protein complexes potentially targeted by Vpr. The proximity interaction network of WT and Q65R Vpr proteins in MG132-treated HEK293 cells (6 hpi) compared to that of WT Vpr in non-MG132-treated HEK293 cells (7 hpi) reveals several interesting complexes potentially targeted by Vpr. Identified subunits of these complexes are highlighted in zoomed boxes, such as APC/C, BASC, CCR4-NOT, PRC, SMN, and ORC. The heat map displays the scaled spectral counts (SC) of preys significantly identified with MG132-treated WT and/or Q65R Vpr baits but not in the untreated WT Vpr control bait. Unidentified preys are in gray, whereas the most abundant preys are in dark purple.

Of the 352 preys identified in our Vpr's proximity interaction network, only a small fraction (~5 to 10%) overlapped with the AP-MS interactome analysis conducted in HEK293 and Jurkat cell lines by the Krogan group (22) (Fig. 1B; Table S2). However, our Vpr's interactome reached a greater (~40%) overlap with a second AP-MS study conducted in the CEM.SS cell line by the Skowronski group (11) (Fig. 1C; Table S2). More precisely, elements of the APC/C, the ORC complex, the RISC-loading complex, and the SMN complex, as well as centrosomal proteins and polymerase components, were found in both our analysis and that by Hrecka et al. (11) (Table S2). Our BioID analyses complement both AP-MS analyses with 200 additional Vpr preys (Table S2). These cross-analyses indicate that proximity labeling allows the identification of new potential Vpr partners/targets that are not detected using conventional pulldown proteomic approaches.

To identify proteins or protein complexes that are potentially degraded by Vpr, we subtracted the WT Vpr proximity interaction network at 7 hpi from both the WT and Q65R Vpr proximity interaction networks identified in condition of proteasome inhibitor (MG-132) treatment (Fig. 2; Table S3). Several proteins and protein complexes were enriched in the presence of MG-132 in both WT and Q65R Vpr proximity interaction networks. Components of the APC/C, including ANAPC1 (APC1), the BRCA1-associated genome surveillance complex (BASC), which is implicated in the recognition and repair of aberrant DNA structures (37), the CCR4-NOT complex, and the polycomb repressive complex (PRC), along with SMN and ORC complexes, were identified under these conditions, suggesting potential targeting of these complexes/networks by Vpr. Interestingly, upon treatment with MG132, the Q65R Vpr proximity interaction network partially overlapped

FIG 1 Legend (Continued)

prevent Vpr-mediated proteasomal degradation, respectively; see Materials and Methods for detailed procedures. A total of 352 SAINT-filtered Vpr proximal partners/targets were identified by bioinformatic analysis in our merged BioID data set. The data set includes two biological replicates for each of the following conditions: HEK293 (6 h, with MG-132), HEK293 (24 h) and HeLa (24 h). Complexes of statistically enriched processes, such as response to DNA damage, cell cycle, RNA processing, and gene expression, are represented in the framed boxes. For the "response to DNA damage" process, proteins which are not part of determined complexes are also represented individually. Interesting complexes, such as APC/C, are surrounded in light gray, with complex core components encircled with brown dashed lines. Baits (Vpr proteins) and preys (proximal partners/targets) are color coded in red and brown, respectively. Previously reported Vpr partners/targets are in yellow. Reported protein-protein interactions are represented by a light gray line. Interaction statistics were determined using SAINTexpress and considered statistically significant based on the following criteria: iProphet protein probability of ≥0.9; number of unique peptides of ≥2; BFDR of ≤0.02. Complete protein identification results can be found in Table S1. (B and C) Data from the Vpr proximity interaction network were cross-analyzed against the results obtained by affinity purification coupled with mass spectrometry (AP-MS) analyses of HIV-1 Vpr (11, 22). (B) Of the 352 proteins identified by BioID, 16 (~4.6%) and 38 (~10.8%), respectively, were found (purple) in the Vpr AP-MS experiment conducted by the Krogan group (22) in HEK293 cells (left pie chart) and in Jurkat cells (right pie chart). (C) One hundred forty (~39.8%) of the proteins identified by BioID were found (purple) in the Vpr AP-MS experiment conducted by the Skowronski group (11) in CEM.SS cells. The proportion of proteins unidentified by AP-MS is represented in yellow. Results of the cross-analyses can be found in Table S2.

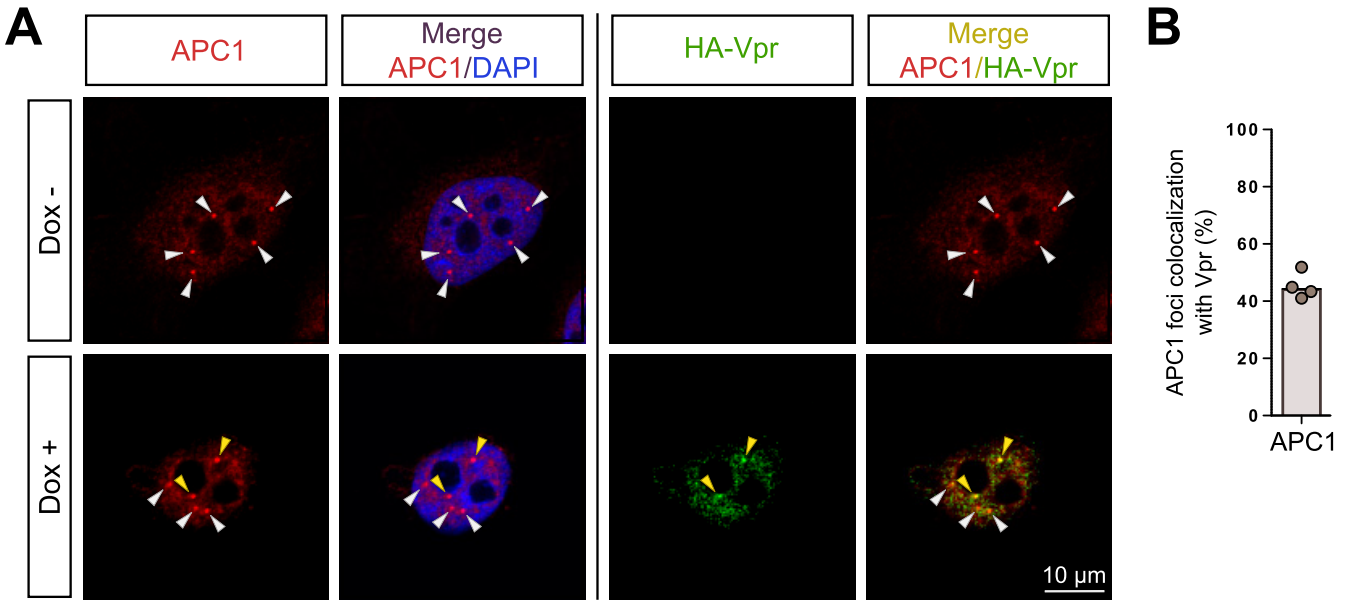

FIG 3 APC1 forms nuclear foci and colocalizes with HIV-1 Vpr. An inducible stable HeLa cell line expressing HA-Vpr Bru was treated for 16 to 18 h with 0.5 μg/ml doxycycline (Dox +) or left untreated (Dox -). APC1 and HA-Vpr were then immunostained using rabbit anti-APC1 and mouse anti-HA primary antibodies. After counterstaining with DAPI (4′,6-diamidino-2-phenylindole), images were acquired by confocal microscopy. (A) Representative images depicting APC1 nuclear staining. APC1 foci are indicated by arrowheads. The colocalization of APC1 with HA-Vpr within nuclear foci is indicated by yellow arrowheads (Dox +; lower panels); white arrowheads indicate APC1 nuclear foci that do not colocalize with HA-Vpr. Bar, 10 μm. (B) The percentage of APC1 foci colocalizing with HA-Vpr was determined on at least a hundred cells (~400 foci) per condition and per replicate. Each dot indicates the average of one biological replicate ($n = 4$). The bar shows the median.

the WT Vpr proximity interaction network, suggesting that some differences could be attributed to the Q65R substitution.

HIV-1 Vpr colocalizes with APC1, a critical scaffolding component of APC/C. Among the complexes identified in our BioID analysis (Fig. 1A and Fig. 2), APC/C drew our attention, given the central role played by this complex in host pathways targeted by Vpr, including cell cycle and DDR/repair regulation (26, 38). To validate a putative proximity interaction of Vpr and APC/C, we assessed the colocalization of APC1, a critical scaffolding component of APC/C (31) identified in the BioID analysis (Fig. 2), and HIV-1 Vpr using a HeLa cell line inducibly expressing hemagglutinin (HA)-tagged Vpr Bru. Interestingly, APC1 is also a component of APC/C that was previously reported to be targeted by viral proteins (39, 40). We first observed that in the absence of Vpr, APC1 has a broad nuclear localization with a staining of the protein in discrete and punctuate nuclear foci (Fig. 3A, Dox -). When Vpr expression was induced, immunostaining revealed an overlap between the Vpr staining and the APC1 foci (Fig. 3A, Dox +). Quantitative colocalization analysis showed that ~44% of the APC1 foci overlapped with the Vpr immunostaining (Fig. 3B). These results indicate that APC1 and Vpr colocalize in discrete nuclear structures, thus validating the bait/prey proximity detected in our BioID analysis and further suggesting a putative interplay between HIV-1 Vpr and APC/C.

HIV-1 Vpr mediates APC1 depletion independently of its ability to induce a G_2/M cell cycle arrest. Vpr mediates the degradation of several cellular proteins, such as UNG2, HLTF, EXO1, and TET2 (11–13, 16, 18). We assessed whether Vpr could mediate the depletion of endogenous APC1 using the Vpr-inducible HeLa cell line described above. As shown in Fig. 4A and B, endogenous APC1 levels were reduced by 30 to 50% when Vpr expression was induced for 24 h. We next validated this observation by transfecting HEK293T cells with a set quantity of a plasmid encoding Flag-APC1 and increasing amounts of a plasmid encoding HA-Vpr. After 2 days, transfected cells were treated with cycloheximide for 6 h to prevent *de novo* protein synthesis and to evaluate the effect of Vpr on the set amount of APC1. As shown in Fig. 4C and D, Flag-APC1 levels were increasingly reduced at increasing HA-Vpr expression levels.

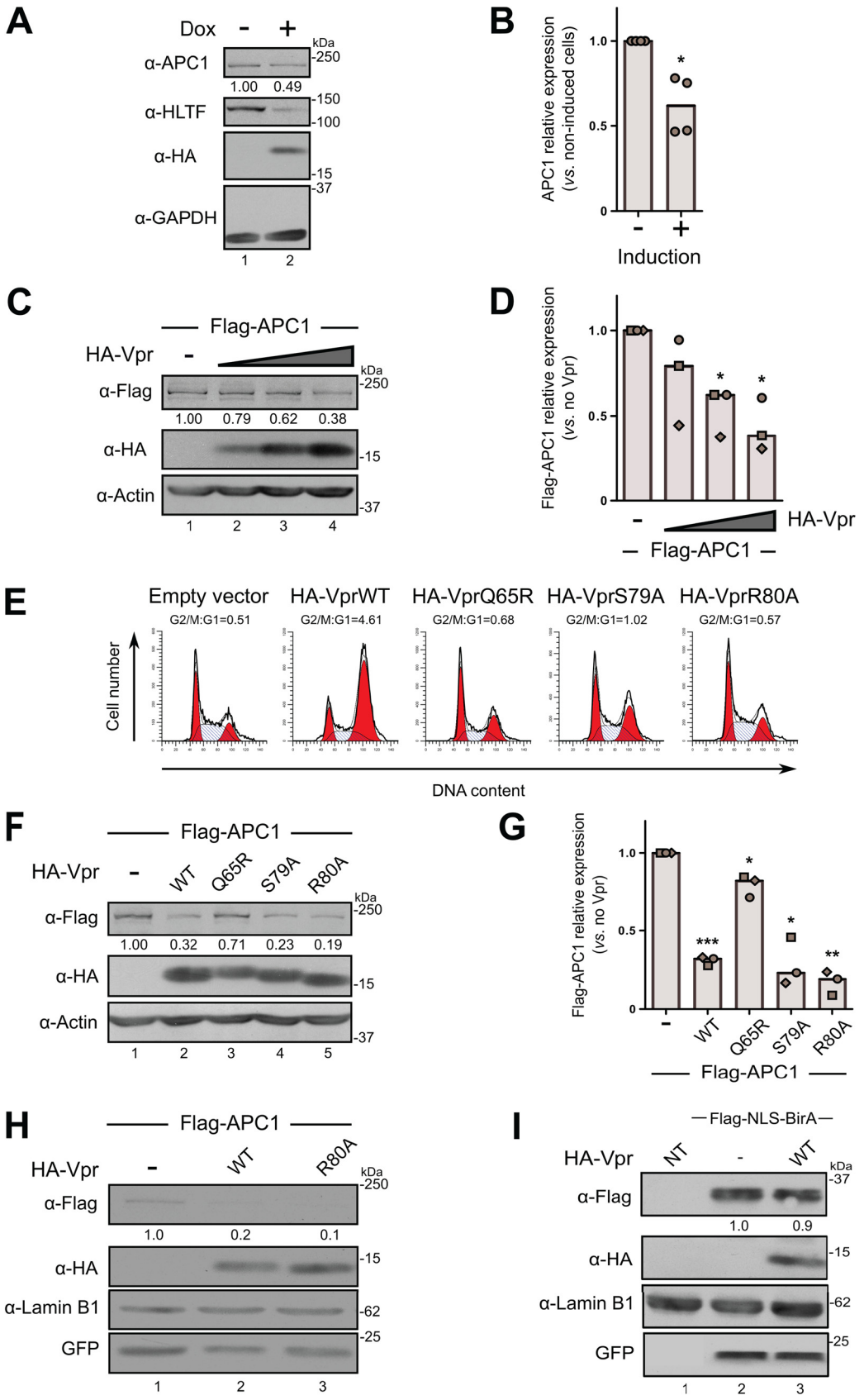

FIG 4 APC1 depletion and G_2/M cell cycle arrest are two independent biological activities of HIV-1 Vpr. (A and B) A stable HeLa cell line inducibly expressing HA-Vpr (Bru) was treated for 24 h with 0.5 μg/ml doxycycline (+; lane 2) or

(Continued on next page)

To ensure that APC1 depletion was not a consequence of Vpr-mediated G_2/M cell cycle arrest, we assessed the effect of well-characterized G_2/M cell cycle arrest-defective Vpr mutants on APC1 levels. We first used the Q65R Vpr mutant, which is well known to be impaired in the recruitment of DCAF1com via DCAF1 and consequently does not arrest cycling cells in G_2/M (Fig. 4E). Whereas WT Vpr induced a strong depletion of APC1, the Q65R mutation in Vpr strongly reduced this effect (Fig. 4F and G, lanes 2 and 3 versus 1). This suggests that Vpr-mediated APC1 depletion requires the recruitment of DCAF1 by Vpr. Interestingly, coexpression of APC1 with either the S79A or R80A mutant of Vpr, which are known to bind DCAF1com but are unable to mediate a G_2/M cell cycle arrest (Fig. 4E), led to an efficient depletion of APC1 (Fig. 4F and G, lanes 4 and 5 versus 1). Similar results were obtained when transfection efficiency was controlled by cotransfecting plasmids encoding Flag-APC1 as well as a construct expressing Vpr (WT or R80A) and GFP (Fig. 4H, lanes 2 and 3 versus 1). Furthermore, expression of Vpr did not affect the expression levels of an irrelevant Flag-NLS-BirA* nuclear protein (Fig. 4I, lanes 3 versus 2), indicating that the effect of Vpr on APC1 was specific. Taken together, these results support the notion that Vpr mediates the depletion of APC1 and further indicate that this activity is not a consequence of the G_2/M cell cycle arrest induced by Vpr.

HIV-1 Vpr relies on a functional DCAF1 complex to degrade APC1 through a proteasomal pathway. Given that the Q65R Vpr mutant is unable to mediate APC1 depletion, we next sought to examine whether DCAF1 was required for Vpr-mediated APC1 depletion using small interfering RNA (siRNA)-directed technology. First, we observed that in the presence of DCAF1 siRNA, Flag-APC1 levels were increased, although the effect was variable and did not reach significance (Fig. 5A and B, lane 3 versus 1), perhaps reflecting difference in transfection efficiency under these conditions. Nevertheless, Vpr was no longer capable of mediating APC1 depletion when DCAF1 was knocked down (Fig. 5A and B, lanes 4 and 3 versus lanes 2 and 1). Furthermore, treatment of transfected cells with MLN4924, a neddylation inhibitor of Cullin-RING E3 ubiquitin ligases, alleviated the Vpr-mediated APC1 depletion (Fig. 5C and D, lanes 4 and 3 versus lanes 2 and 1), suggesting that DCAF1com needs to be neddylated in order to deplete APC1 in the presence of Vpr. To evaluate whether Vpr mediates APC1 depletion by a proteasome-dependent degradation process, similar experiments were conducted in the presence or absence of MG-132. Treatment of cells expressing HA-Vpr and Flag-APC1 with MG-132 limited the extent of APC1 depletion by Vpr (Fig. 5E and F, lanes 4 and 3 versus lanes 2 and 1). Indeed, the inhibition of Vpr-mediated APC1 degradation by MG-132 was comparable to that observed with HLTF, a known Vpr target degraded through the proteasomal pathway (Fig. 5E and F, lanes 8 and 7 versus lanes 6 and 5) (11, 12), although in the case of HLTF, the cycloheximide

FIG 4 Legend (Continued)
left untreated (−; lane 1). Endogenous APC1, HLTF, and HA-Vpr expression levels were analyzed by immunoblotting. A representative Western blot is presented (A), and quantification of four biological replicates is depicted (B). (C and D) HEK293T cells (4.5×10^6) were transfected with 5 μg of plasmid encoding Flag-APC1 and an empty control vector (lane 1) or with increasing amounts of a plasmid encoding HA-Vpr (1 μg, 2.5 μg, or 5 μg; lanes 2 to 4). At 42 h posttransfection, cells were treated with 20 μg/ml cycloheximide for 6 h and analyzed for Flag-APC1 and HA-Vpr levels by Western blotting. A representative Western blot is presented (C), and quantification of three biological replicates is depicted (D). (E) HEK293T cells were transfected with 2.5 μg of the indicated Vpr-expressing or control plasmids and 1 μg of a construct encoding GFP. Two days later, the cell cycle profiles of GFP^+ cells were analyzed by flow cytometry. G_2/M-to-G_1 ratios were calculated and are indicated above each histogram. (F and G) HEK293T cells were cotransfected with 5 μg of a plasmid encoding Flag-APC1 and 5 μg of an empty vector (lane 1) or 5 μg of a plasmid encoding HA-Vpr WT or Q65R, S79A, and R80A mutants (lanes 2 to 5) and processed as described for panel C. A representative Western blot is presented (F), and quantification of three biological replicates is depicted (G). (H and I) HEK293T were cotransfected with 5 μg of a plasmid encoding Flag-APC1 (H) or Flag-NLS-BirA* (I) and 5 μg of WPI lentiviral vector encoding GFP as well as HA-Vpr WT (H and I) or VprR80A (H) or GFP alone (H and I) and processed as described for panel C. (A, C, F, H, and I). Endogenous APC1 and Flag-APC1 were quantified by using ImageJ and by calculating the intensity of the APC1 bands relative to the loading control (A, C, and F) or GFP (H and I). The value obtained with the APC1 control was set at 1.0, as indicated below the upper panels. (B, D, and G) Each dot indicates APC1 relative expression of one biological replicate ($n = 3$ or 4). Bars represent the medians. Statistically significant differences (*, $P \leq 0.05$; **, $P \leq 0.01$; ***, $P \leq 0.001$) relative to the no-Vpr control were determined by two-tailed paired Student's t test.

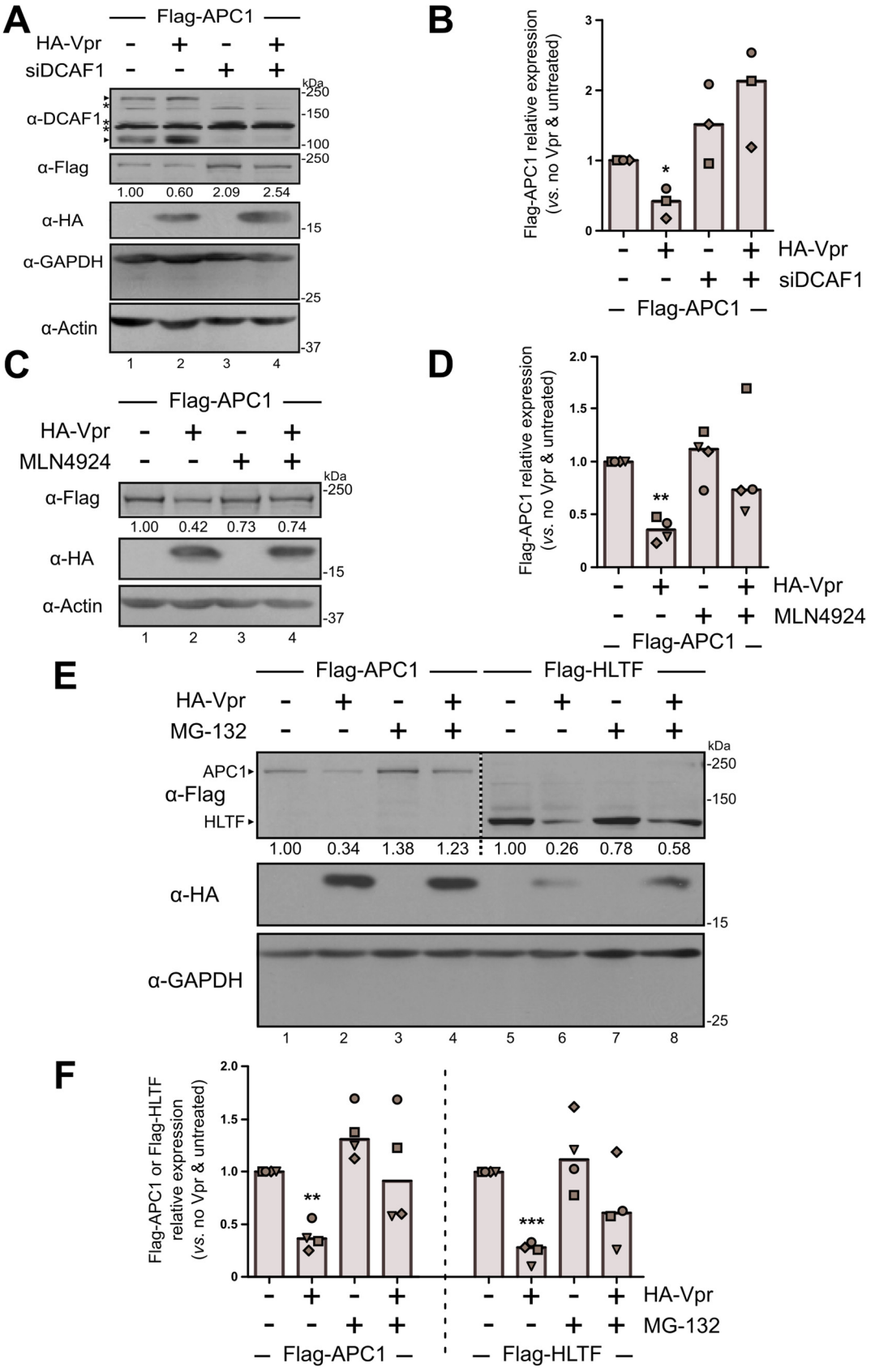

FIG 5 HIV-1 Vpr Induces APC1 degradation through a process that requires DCAF1com and a functional proteasome. (A and B) HEK293T were transfected with DCAF1 siRNA (siDCAF1; lanes 3 and 4) or scrambled siRNA (lanes 1 and 2) and

(Continued on next page)

treatment might have limited the rescue by MG-132. Altogether, these results indicate that Vpr mediates APC1 degradation through a mechanism that requires the recruitment of an active DCAF1com by Vpr and the presence of a functional proteasome.

HIV-1 Vpr forms a physical complex with APC/C independently of DCAF1. We next assessed whether Vpr and APC1 can be found in the same complex and if the association between the two proteins was influenced by the presence of DCAF1. To do so, HEK293T cells were transfected with plasmids encoding Flag-APC1 and HA-Vpr (WT or Q65R), and proteins coimmunoprecipitated with HA-Vpr were then analyzed for the presence of Flag-APC1 and/or DCAF1 by immunoblotting. Despite efficient DCAF1 coimmunoprecipitation with WT Vpr (Fig. 6A, lanes 3 and 4 versus 1), we were unable to detect a specific coimmunoprecipitation of APC1 under these conditions (lane 4 versus 2). In clear contrast, we detected APC1 in the Q65R Vpr mutant immunoprecipitates (Fig. 6A, lane 7 versus lanes 6 and 2), suggesting that the degradation of APC1 mediated by WT Vpr limits the detection of Vpr-APC1 complexes. To further support these findings, we performed the WT Vpr pulldown in cells where DCAF1 expression was knocked down by siRNA to prevent Vpr-mediated APC1 degradation. In this context, APC1 was enriched in complexes that coprecipitated with WT Vpr (Fig. 6A, lane 5 versus lanes 4 and 2). Overall, these results suggest that Vpr forms a physical complex with APC1 to mediate its degradation by the proteasome. Although DCAF1com is required for Vpr-mediated degradation of APC1, association of Vpr to APC1 can occur independently of DCAF1com recruitment by Vpr.

It was reported previously that APC1 forms a complex with either Cdh1 or Cdc20, two APC/C coactivators that allow selective substrate recognition (26). Given this context, we next asked if APC/C regulatory components could be found in complex with Vpr. To this end, Myc-tagged APC/C coactivators were expressed either with WT Vpr or the Q65R Vpr mutant and processed for HA or Myc pulldowns followed by analysis of the immunocomplexes for the presence of HA-Vpr, Myc-Cdh1/Myc-Cdc20, and DCAF1 by immunoblotting. Cdh1 was enriched in the coimmunoprecipitate with WT Vpr (Fig. 6B, lane 6 versus 4), while both coactivators were found to associate with the Q65R mutant of Vpr (lane 8 versus lane 4 and lane 9 versus lane 5), indicating that APC/C coactivators and Vpr can form a complex. Endogenous DCAF1 was also detected in the immunoprecipitates of WT Vpr but not in those of the Q65R mutant (Fig. 6B, lanes 2, 6, and 7 versus lanes 3, 8, and 9). Moreover, upon immunoprecipitation of Cdh1, both WT and Q65R Vpr proteins were coimmunoprecipitated (Fig. 6B, lanes 6 and 8 versus 4), yet only a trace of Q65R Vpr, and not WT Vpr, could be detected upon immunoprecipitation of Cdc20 (Fig. 6B, lanes 9 and 7 versus 5). These results suggest that Cdh1, which is part of distinct APC/C complexes, can preferentially associate with Vpr, perhaps reflecting a specific targeting of APC/C^{Cdh1} by Vpr or increased stability of the Vpr-APC/C^{Cdh1} complex compared to Vpr-APC/C^{Cdc20}. Together, these results support the notion that Vpr forms a complex with components of the APC/C complex, including APC1 as

FIG 5 Legend (Continued)
incubated overnight. Cells were then transfected with 5 μg of a plasmid encoding Flag-APC1 and 5 μg of either an empty vector (lanes 1 and 3) or a plasmid encoding HA-Vpr (lanes 2 and 4). At 42 h after plasmid transfection, cells were processed as described for Fig. 4 and analyzed for Flag-APC1, HA-Vpr, and DCAF1 levels by Western blotting. A representative Western blot is presented (A), and quantification of three biological replicates is depicted (B). Arrowheads indicate DCAF1-related bands that were depleted by the siRNA-DCAF1 while asterisks indicate nonspecific bands. (C and D) HEK293T were transfected with plasmids as for panels A and B and treated 42 h after transfection with 20 μg/ml cycloheximide and 1 μM MLN4924 (lanes 3 and 4) or an equivalent volume of DMSO (lanes 1 and 2) for 6 h. Flag-APC1 and HA-Vpr levels were monitored by Western blotting. A representative Western blot is presented (C), and quantification of four biological replicates is depicted (D). (E and F) Cells were transfected and treated as described for panels C and D, except that 10 μM MG-132 was used instead of MLN4924. As controls, 5 μg of a plasmid encoding Flag-HLTF was transfected with 5 μg of an empty vector or a construct expressing HA-Vpr. After 42 h, transfected cells were treated as indicated above. A representative Western blot is presented (E), and quantification of four biological replicates is depicted (F). (A, C, and E) Quantifications were determined as described for Fig. 4. (B, D, and F). For panel B, both GAPDH and actin were used as loading controls in the quantifications and showed similar results. Each dot indicates Flag-APC1 or Flag-HLTF relative expression for one biological replicate ($n = 3$ or 4). Bars represent the medians. Statistically significant differences (*, $P \leq 0.05$; **, $P \leq 0.01$; ***, $P \leq 0.001$) relative to the no-Vpr control were determined by two-tailed paired Student's *t* test.

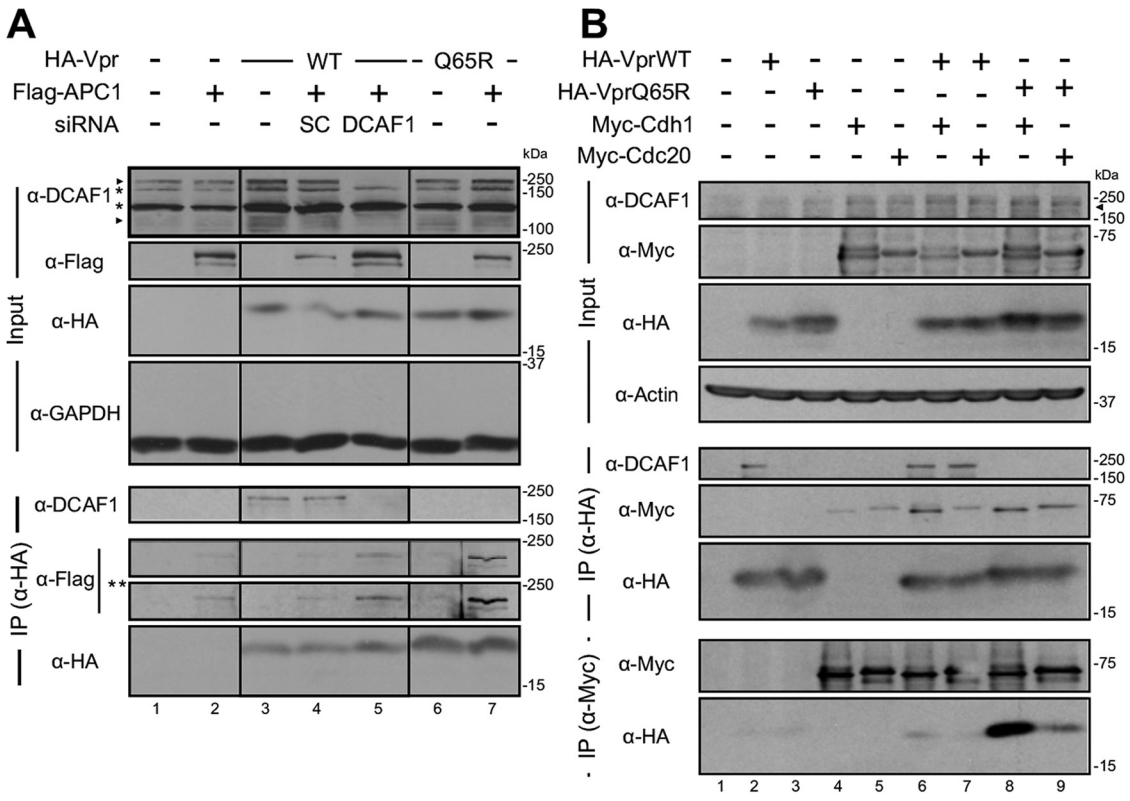

FIG 6 HIV-1 Vpr forms a physical complex with APC/C independently of DCAF1com. (A) HEK293T were transfected with siRNA-DCAF1 (DCAF1; lane 5) or siRNA-scrambled (SC; lane 4) or mock transfected (lanes 1 to 3, 6, and 7). Following an overnight incubation, cells were transfected with 10 μg of a plasmid encoding Flag-APC1 (lanes 2, 4, 5, and 7) and 10 μg of a plasmid encoding either HA-VprWT (lanes 3 to 5) or HA-VprQ65R (lanes 6 and 7). Two days later, cells were harvested and lysed in ice-cold Triton lysis buffer. Lysates were then incubated with HA beads for 3 h. Flag-APC1, HA-Vpr, and DCAF1 levels were determined by immunoblotting in both the input and immunoprecipitated fractions. Arrowheads indicate the DCAF1 bands that were depleted by the siRNA-DCAF1, while single asterisks indicate nonspecific bands, and the double asterisk indicates a long exposure of the blot probed with the anti-Flag antibody. (B) HEK293T cells were transfected with 10 μg of a plasmid encoding either Myc-Cdh1 (lanes 4, 6, and 8) or Myc-Cdc20 (lanes 5, 7, and 9) and either HA-VprWT (lanes 2, 6, and 7) or HA-VprQ65R (lanes 3, 8, and 9). Two days posttransfection, cells were harvested and lysed in ice-cold Triton lysis buffer. Lysates were then incubated with anti-HA beads for 3 h or with a rabbit anti-Myc antibody for 2 h followed by an additional hour with protein A-Sepharose beads. Myc-Cdh1, Myc-Cdc20, HA-Vpr, and DCAF1 levels were determined by immunoblotting in both the input and immunoprecipitated fractions.

well as the coactivators Cdh1 and to a lesser extent Cdc20, and is likely to affect the integrity of APC/C complexes by mediating the degradation of at least APC1.

HIV-1 Vpr of transmitted/founder primary isolates mediate APC1 degradation. In a recent SILAC (stable isotope labeling by amino acids in cell culture) analysis, the Lehner group reported that NL4.3 Vpr expression has a broad modulatory effect on the cellular proteome (23). Surprisingly, no components of the APC/C complex were found to be modulated by Vpr in this analysis. To confirm that the APC1 degradation mediated by Vpr was specific to the HIV-1 Bru strain used herein, we analyzed side-by-side the impact of two other Vpr variants from laboratory-adapted HIV-1 (Lai and NL4.3) on APC1 levels using our transient-expression system in HEK293T cells. Strikingly and in clear contrast to both Bru and Lai variants, NL4.3 Vpr was unable to mediate APC1 degradation, while all three Vpr variants were capable of mediating HLTF degradation (Fig. 7A and B, lane 4 versus lanes 2 and 3). These results indicate that Vpr variants display differences in their ability to mediate APC1 degradation and importantly further demonstrate that Vpr-mediated APC1 degradation is not involved in the induction of G_2/M cell cycle arrest, since both Vpr variants from Bru (Fig. 4E) and NL4.3 (4) can trigger a cell cycle arrest in G_2/M.

Given that the Vpr variants tested previously originated from laboratory-adapted HIV-1, we next sought to confirm that Vpr variants encoded by transmitted/founder

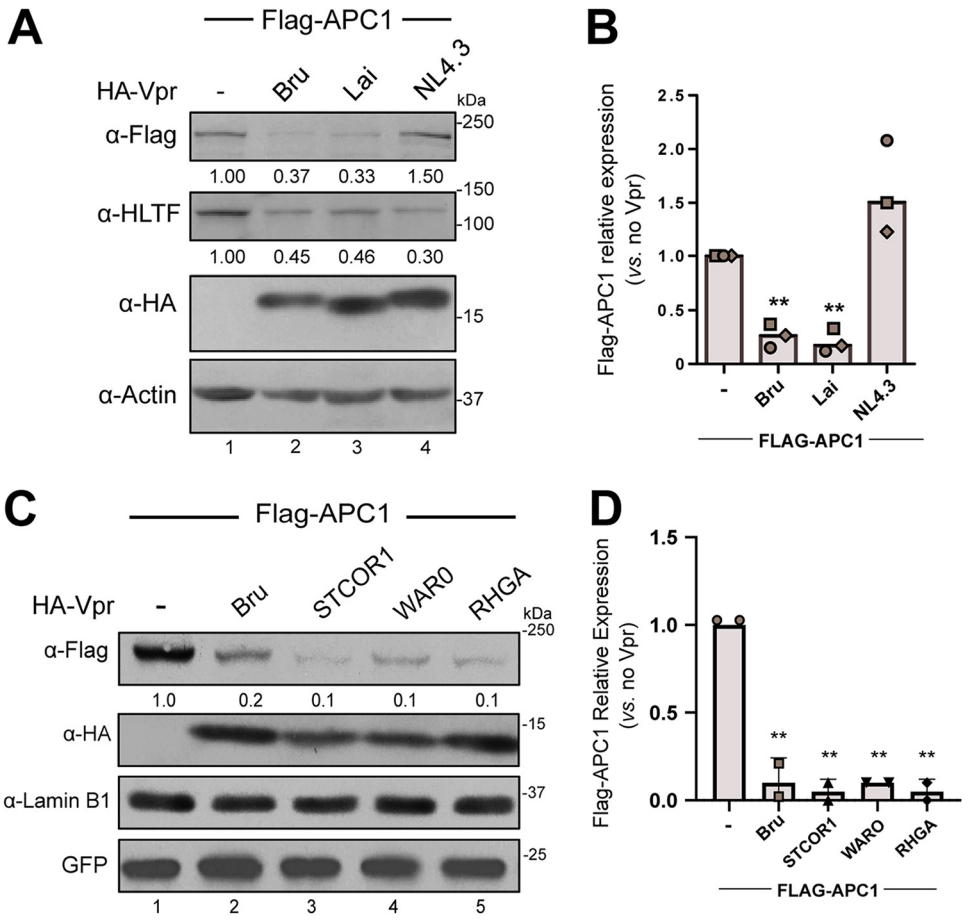

FIG 7 HIV-1 Vpr primary variants mediate APC1 degradation. (A and B) HEK293T cells were transfected with 5 μg of a plasmid encoding Flag-APC1 (lanes 1 to 4) and 5 μg of either an empty vector (lane 1) or a plasmid encoding the indicated HA-Vpr variants (lanes 2 to 4). After 42 h, cells were treated as described for Fig. 4 and processed for immunoblotting. A representative Western blot is presented (A), and quantification of three biological replicates is depicted (B). (C and D) HEK293T cells were transfected with 5 μg of a plasmid encoding Flag-APC1 (lanes 1 to 5), 5 μg of an empty vector (lane 1), or a plasmid encoding the indicated HA-tagged Vpr proteins (lanes 2 to 5) and 1 μg of a plasmid encoding GFP for 42 h, treated as described for Fig. 4, and processed for immunoblotting. A representative Western blot is presented (C), and quantification of two biological replicates is depicted (D). (A and C) Quantifications were determined as described for Fig. 4. (B and D) Each dot indicates Flag-APC1 relative expression of one biological replicate ($n = 2$ or 3). Bars represent the medians. Statistically significant differences (**, $P \leq 0.01$) relative to the no-Vpr control were determined by two-tailed paired Student's *t* test.

primary isolates (RHGA, STCOr1, and WAR0) were able to mediate APC1 degradation (41). Vpr variants encoded by these three primary isolates mediated APC1 degradation (Fig. 7C and D, lanes 3 to 5 versus 1). These results indicate that Vpr-mediated APC1 degradation activity is not restricted to laboratory-adapted Vpr variants but is conserved by several primary variants of Vpr, highlighting the potential relevance of this interplay in HIV-1 pathogenesis.

The N28S-G41N double substitution impedes HIV-1 Vpr ability to mediate APC1 degradation. Given that NL4.3 Vpr does not mediate APC1 degradation, we next aligned its amino acid sequence with its counterpart from Bru Vpr. We found only three divergent amino acid residues between Vpr variants Bru and NL4.3, namely, H15Y, N28S, and G41N (Fig. 8A). We generated these individual substitutions as well as combinations of these in the corresponding amino acid positions in the Bru Vpr variant and analyzed their impact on Vpr ability to mediate APC1 degradation. None of the individual substitutions completely abolished Vpr-mediated APC1 degradation (Fig. 8B and C, lanes 3 to 5 versus lanes 1 and 6). In clear contrast, combining substitutions at amino acids 28 and 41, namely, N28S and G41N, strongly impaired Vpr-mediated APC1

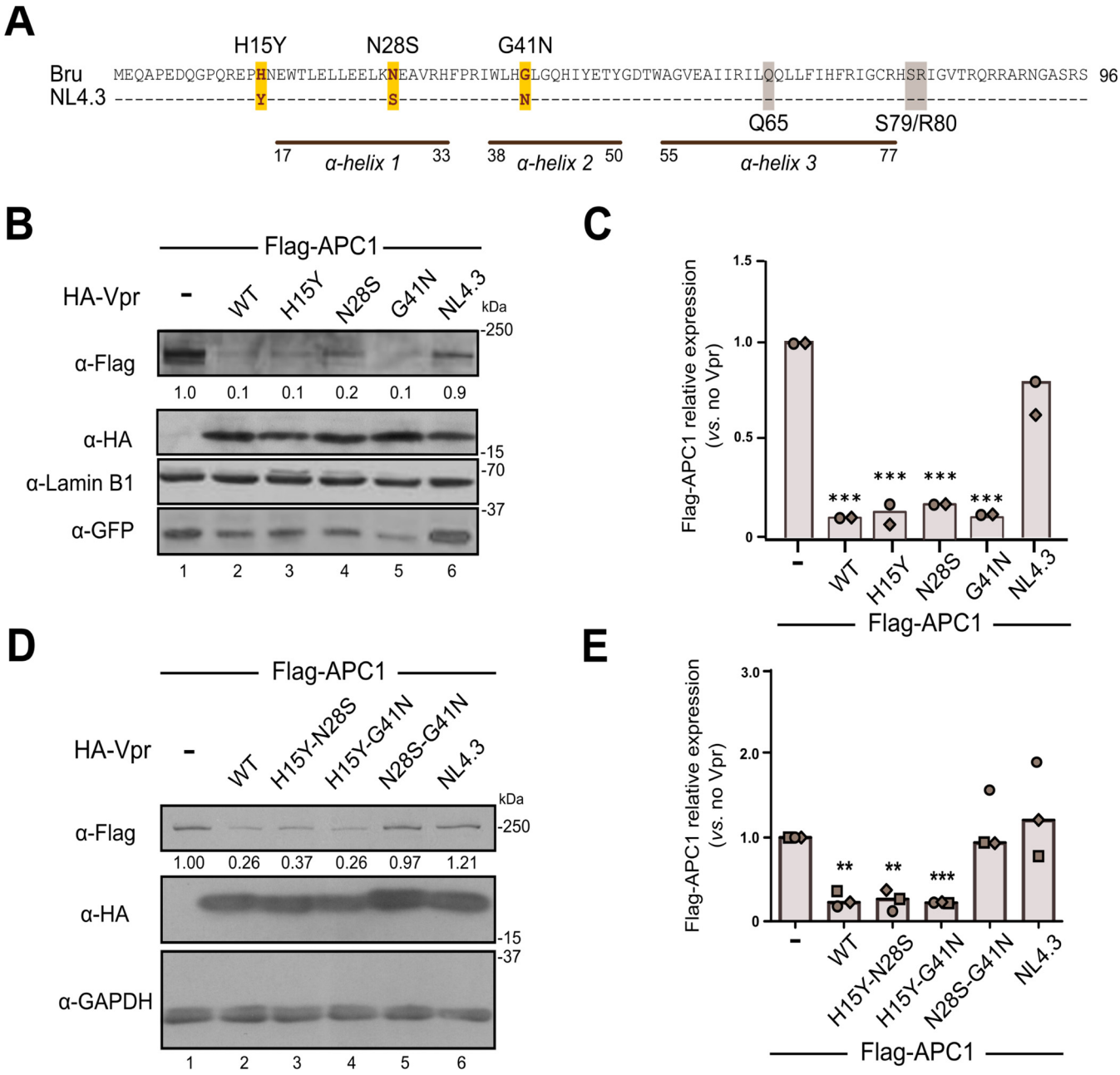

FIG 8 The double substitution N28S-G41N in Vpr impedes its ability to mediate APC1 degradation. (A) Sequences from Bru and NL4.3 Vpr variants were aligned using Clustal Omega. Amino acid positions (15, 28, and 41) that are not conserved between variants are highlighted in yellow. Residues known to be important for Vpr activities (Q65, S79, and R80) are highlighted in gray. (B and C) HEK293T cells were transfected with 5 μg of a plasmid encoding Flag-APC1 (lanes 1 to 6), 5 μg of either an empty vector (lane 1) or a plasmid encoding the indicated HA-tagged Vpr (lanes 2 to 6), and 1 μg of a plasmid encoding GFP. After 42 h, cells were treated as described for Fig. 4. A representative Western blot is presented (B), and quantification of two biological replicates is depicted (C). (D and E) HEK293T cells were transfected with 5 μg of plasmid encoding Flag-APC1 (lanes 1 to 6) and 5 μg of either an empty vector (lane 1) or a plasmid encoding the indicated HA-tagged Vpr (lanes 2 to 6). Cells were processed as described for panels B and C). A representative Western blot is presented (D), and quantification of three biological replicates is depicted (E). (B and D) Quantifications were determined as described for Fig. 4. (C and E) Each dot indicates Flag-APC1 relative expression of one biological replicate ($n = 2$ or 3). Bars represent the medians. Statistically significant differences (**, $P \leq 0.01$; ***, $P \leq 0.001$) relative to the no-Vpr control were determined by two-tailed paired Student's t test.

degradation; in fact, this mutant mimicked the NL4.3 Vpr variant phenotype (Fig. 8D and E, lane 5 versus lanes 1 and 6). These results delineate Vpr residues N28 and G41 as critical for Vpr ability to mediate APC1 degradation.

In order to evaluate the possibility that Vpr from other HIV-1 strains could mediate APC1 degradation, we took advantage of the HIV Sequence Database (Los Alamos National Laboratory; http://www.hiv.lanl.gov/) and analyzed 4,835 HIV-1 Vpr variants. We observed

that amino acids N28 and G41 were conserved in ~32.1% and ~60.9%, respectively, of the Vpr variants, suggesting that a significant number of HIV-1 strains encode Vpr variants potentially capable of inducing APC1 degradation.

NL4.3 Vpr does not interact efficiently with APC1 yet colocalizes with APC1 nuclear foci. Given that NL4.3 Vpr is unable to mediate the degradation of APC1, we next determined whether this defect resulted from a binding impairment. To do so, we transfected HEK293T cells with plasmids encoding NL4.3 Vpr or Vpr Q65R Vpr (Bru variant), a mutant that does not degrade APC1 but efficiently forms a complex with the protein, and analyzed APC1 levels in the Vpr immunoprecipitate. NL4.3 Vpr was less effective at forming a complex with APC1 than Bru Vpr Q65R (Fig. 9A, lane 2 versus lane 4; Fig. 9B). Indeed, quantification of the binding efficiency revealed that NL4.3 Vpr displayed a reduction of approximately 80% compared to BruVprQ65R, suggesting that the three amino acid residues at positions 15, 28, and 41, which distinguish NL4.3 Vpr from Bru Vpr, are likely to play an important role in the formation of a complex with APC1.

To assess whether the reduction in efficiency of binding of NL4.3 Vpr to APC1 impacted their colocalization, we coexpressed Flag-APC1 with HA-tagged NL4.3 Vpr or Bru Vpr in HeLa cells and analyzed their colocalization. Despite defective binding to APC1, NL4.3 Vpr colocalized with APC1 nuclear foci as efficiently as did Bru Vpr (Fig. 9C and D), suggesting that such a colocalization is not dictated solely by the physical interaction of the two proteins.

The HIV-1 harboring the Vpr N28S-G41N double substitution does not impact HIV-1 replication in primary CD4$^+$ T cells and macrophages. Having identified amino acid substitutions that abrogate APC1 degradation by Vpr, we next assessed the impact of these substitutions on HIV-1 replication in activated primary CD4$^+$ T cells and primary monocyte-derived macrophages (MDMs). The N28S and G41N substitutions were introduced by site-directed mutagenesis in the CCR5-tropic HxBru-ADA-GFP infectious molecular clone (42), and the resulting viruses were validated for Vpr's ability to mediate a G_2/M cell cycle arrest during infection of the MT4 T cell line. As shown in Fig. 10A, vesicular stomatitis virus G glycoprotein (VSV-G)-pseudotyped viruses expressing either WT or N28S-G41N double-substitution Vpr proteins induced a strong G_2/M cell cycle arrest of similar efficiency (G_2/M-to-G_1 ratio of 1.51 versus 1.65), in contrast to the Vpr-deficient virus control (G_2/M-to-G_1 ratio of 0.81). This indicates that the proteins were expressed and further confirms that Vpr mutations that abrogate APC1 degradation do not impact Vpr-mediated G_2/M cell cycle arrest during HIV-1 infection of MT4 cells.

We then infected activated primary CD4$^+$ T cells at different multiplicities of infection and followed the replication of the viruses over 6 days (Fig. 10B). As indicated by the percentage of GFP$^+$ cells, expression of Vpr did not confer any detectable replicative advantage in primary CD4$^+$ T cells, as previously reported (43). In fact, the three isogenic viruses displayed very similar spreading of infection in these cells, indicating that expression of neither the WT nor the N28S-G41N Vpr mutant had any impact on HIV-1 replication in this system.

Last, we tested the effect of the N28S-G41N double substitution on viral replication in MDMs, a system where expression of Vpr was reported to provide a replication advantage to HIV-1 (17). While the virus encoding WT Vpr did spread more efficiently than the Vpr-deficient virus in MDMs from four of five donors, no difference in replication kinetics was observed between the WT HxBru-ADA-GFP and the Vpr double mutant virus (Fig. 10C and D). Furthermore, at 3 days after infection, we assessed Vpr expression levels in infected MDMs by flow cytometry. In clear contrast to the Vpr-deficient virus, we detected a Vpr signal for both the WT and the Vpr double-mutant viruses, indicating that these viruses properly expressed a functional Vpr (Fig. 10E). Altogether, these results indicate that mutations abrogating Vpr-mediated APC1 degradation do not impede HIV-1 replication in primary CD4$^+$ T cells or macrophages, suggesting that the interplay between HIV-1 Vpr and APC/C might influence other aspects of HIV-1 pathogenesis.

DISCUSSION

Many studies have employed proteomic approaches to define the HIV-1 Vpr interactome and ultimately identify Vpr partners/targets. Both the Krogan and the Skowronski

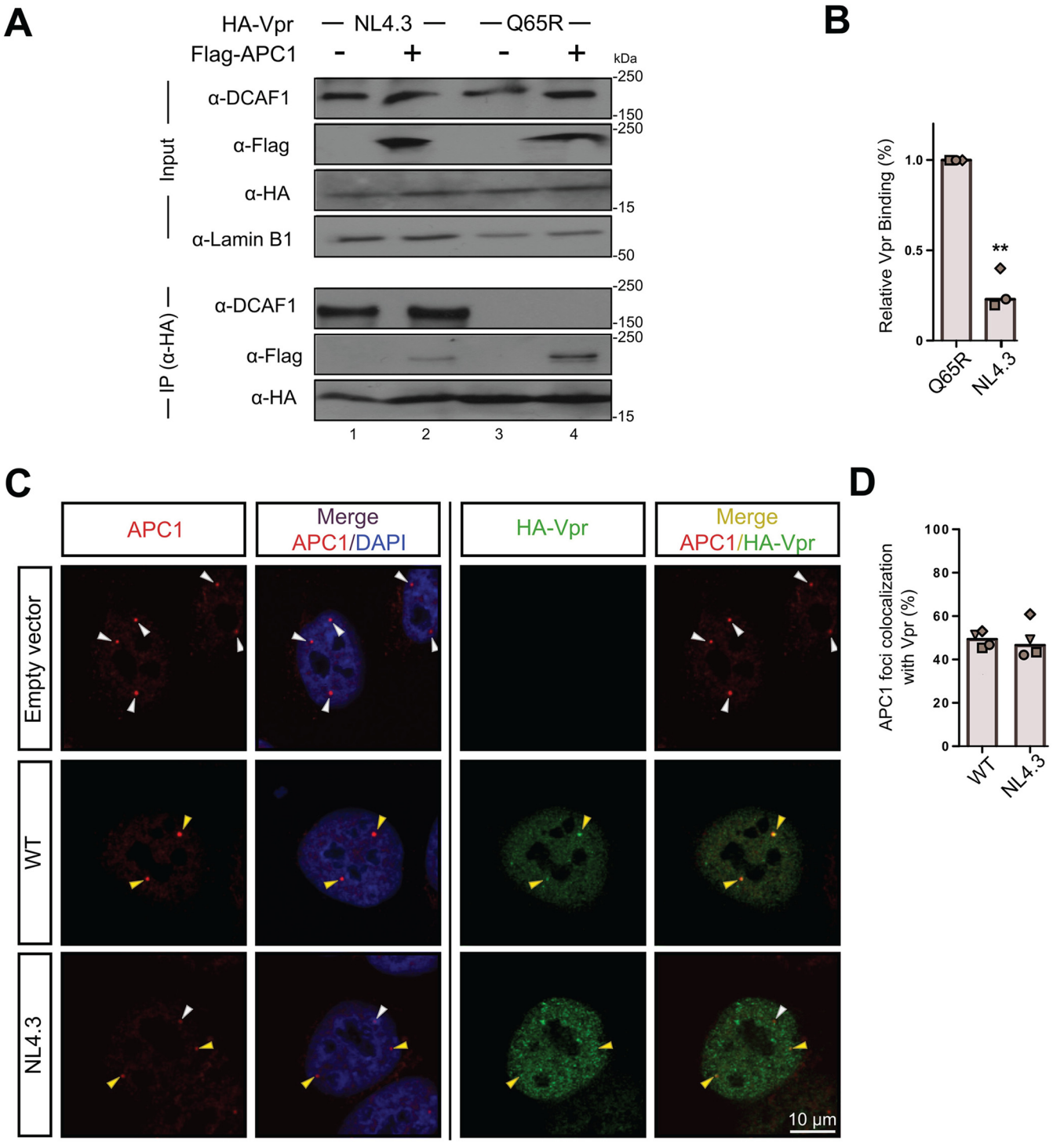

FIG 9 NL4.3 Vpr is less efficient at forming a complex with APC1. (A) HEK293T cells were transfected with 10 μg of a plasmid encoding Flag-APC1 (lanes 2 and 4) and 10 μg of a plasmid encoding either NL4.3 HA-Vpr (lanes 1 and 2) or Bru HA-VprQ65R (lanes 3 and 4). Two days later, cells were processed and immunoprecipitation with anti-HA antibodies was performed as for Fig. 6. Flag-APC1, HA-Vpr, and DCAF1 levels were determined by immunoblotting in both the input and immunoprecipitated fractions. (B) Flag/HA ratios from coimmunoprecipitated proteins (A) were determined and normalized to VprQ65R. Each dot indicates the data for one biological replicate ($n = 3$). Bars represent the medians. (C and D) HeLa cells were transfected with plasmids encoding the indicated HA-Vpr (NL4.3 or Bru [WT]) or an empty vector. At 24 h posttransfection, cells were stained as described for Fig. 3. (C) APC1 foci are indicated by arrowheads. Colocalization of APC1 with HA-Vpr within nuclear foci is indicated by yellow arrowheads; white arrowheads indicate APC1 nuclear foci that do not colocalize with HA-Vpr. Bar, 10 μm. (D) The percentage of APC1 foci colocalizing with HA-Vpr was determined on at least a hundred foci per condition and per replicate. Each dot indicates the average for one biological replicate ($n = 4$). Bars represent the medians. Statistically significant differences (**, $P \leq 0.01$) relative to the no-Vpr control were determined by two-tailed paired Student's *t* test.

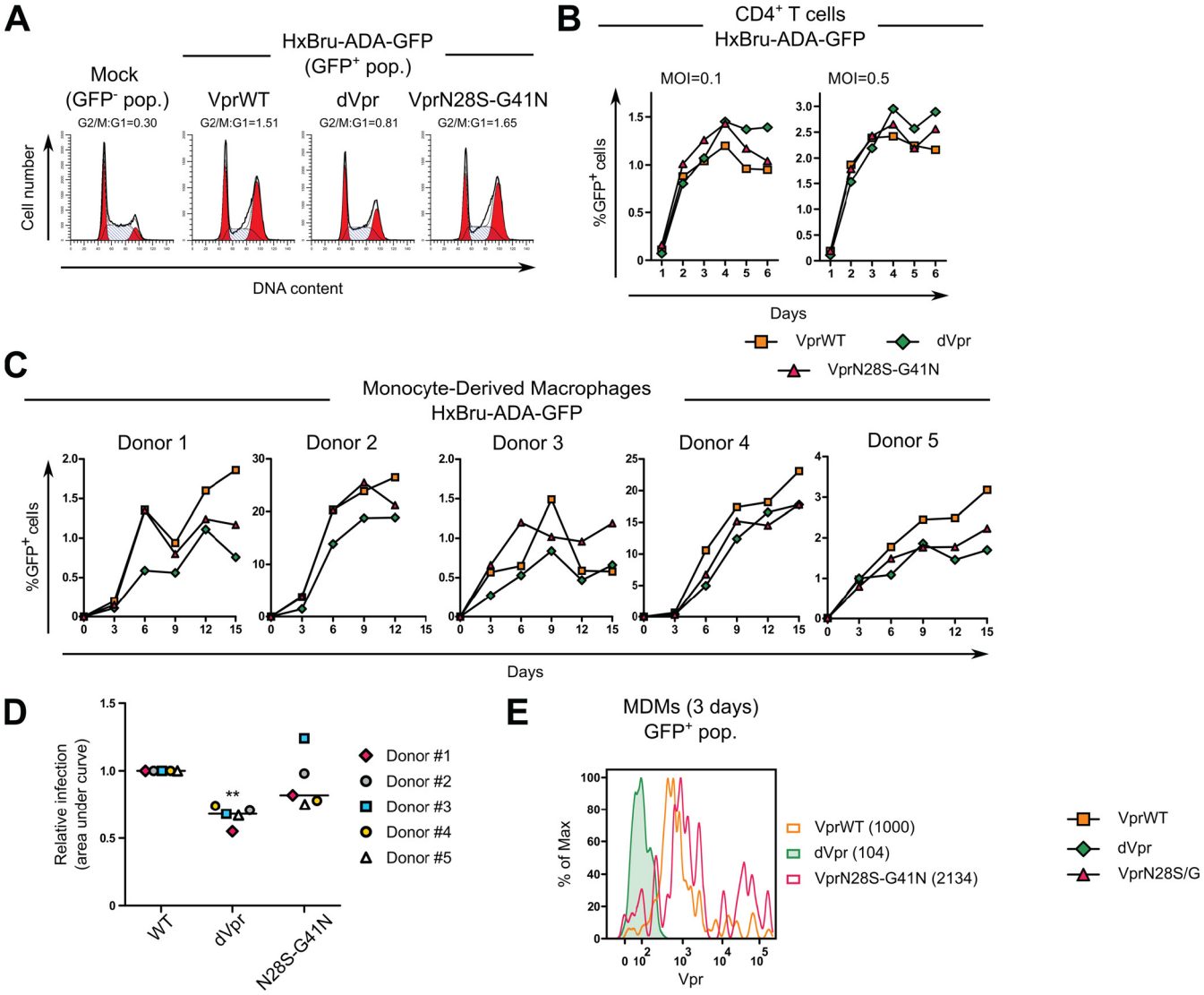

FIG 10 The HIV-1 Vpr double substitution N28S-G41N does not affect HIV-1 replication in primary CD4$^+$ T cells or macrophages. (A) MT4 cells were infected with VSV-G-pseudotyped HxBru-ADA-GFP viruses, expressing the indicated Vpr, at an MOI of 0.75 or mock infected. Twenty-four hours later, cells were harvested and the cell cycle profile of the indicated population (GFP$^-$ or GFP$^+$) analyzed. G_2/M-to-G_1 ratios were calculated and are indicated above each histogram. (B) Activated primary CD4$^+$ T cells were infected with VSV-G-pseudotyped HxBru-ADA-GFP viruses expressing the indicated Vpr, at MOI of 0.1 and 0.5. The percentage of GFP$^+$ cells was monitored daily for up to 6 days postinfection by flow cytometry. (C) Primary MDMs were infected with VSV-G-pseudotyped HxBru-ADA-GFP viruses, expressing the indicated Vpr, at an MOI of 1 for up to 15 days postinfection. Viral spread was monitored every 3 days by determining the percent GFP$^+$ cells by flow cytometry. (D) The area under the curve for each condition from donors in panel C was determined using GraphPad Prism and the relative infection spread for each condition calculated by setting the data obtained for individual donor infected with HxBru-ADA-GFP VprWT virus to 1. **, $P \leq 0.01$ (statistically significant difference between HxBru-ADA-GFP dVpr and both WT and N28S-G41N Vpr viruses as determined by two-tailed Mann-Whitney test). (E) Primary MDMs were infected as for panel C. Three days later, Vpr expression levels were assessed in the GFP$^+$ population by flow cytometry. Mean fluorescence intensities are given in parentheses.

groups analyzed the Vpr interactome by using AP-MS in both HEK293 and Jurkat cells (22) and in CEM.SS cells (11), respectively, leading to the identification of new Vpr partners/targets, including HLTF (11). More recently, the impact of HIV-1 infection and specifically of Vpr on the cellular proteome was analyzed, using a SILAC approach, by the Margottin-Goguet group using HeLa cells (12), and more extensively by the Lehner group using CEM T4 cells (23). Indeed, the latter study identified almost 2,000 proteins that are directly or indirectly modulated by Vpr during HIV-1 infection (23). Both approaches are complementary, since, for instance, Jäger et al. (22) identified the SMN complex as a potential Vpr partner/target by AP-MS, while Greenwood et al. (23) successfully demonstrated the ability of Vpr to deplete components of the SMN complex by SILAC and more conventional

biochemical approaches. Furthermore, Hrecka et al. (11) and Lahouassa et al. (12) used AP-MS and SILAC, respectively, to identify HLTF as a Vpr target.

However, given the nature of the approach used to discover partners/targets, transient or unstable interactions of proteins or protein complexes with Vpr are likely to have been missed, suggesting that the Vpr interaction network is most probably underestimated. To further define such a network and identify novel Vpr targets/partners, we used the BioID proximity labeling approach (25). A major strength of BioID is to provide *in cellulo* tagging of not only stable but also weak and transient proximal interactors and to allow their identification, following harsh cell lysis conditions, by mass spectrometry. Using this approach with WT Vpr and the well-characterized Q65R and R80A Vpr mutants, we uncovered 352 preys (Fig. 1A and Table S1), including well-characterized Vpr partners such as DCAF1 and DDB1 (5–7), as well as individually characterized targets such as UNG (16), EXO1 (13), or complexes like the RISC loading complex (32) and the SMN complex (22, 23). Of the 352 preys, 152 were found in AP-MS analyses reported by the Krogan group (22) or the Skowronski group (11), leading to the identification of 200 new proteins that were previously not detected (Fig. 1B and C; Table S2). Analysis of the Vpr interaction network revealed that in addition to being in close proximity to components involved in DNA damage and cell cycle processes, Vpr interacted with proteins implicated in centrosome regulation, RNA processing, and gene expression (Fig. 1A and Table S1), as reported by previous studies (18, 19, 22, 23, 44, 45).

More recently, the Bieniasz group analyzed the Vpr proximity interaction network in MT4 cells using BioID and reported the identification of a chromosome periphery protein, CCDC137/cPERP-B, as a novel target of Vpr, whose depletion induced G_2/M cell cycle arrest and enhanced HIV gene expression (46). Analysis of the Vpr proximity interactome generated from the Bieniasz study with our data revealed an overlap of only 7 proteins, namely, CCNT1, EZH2, FAM208A, JMJD1C, MEPCE, PPM1G, and ZBTB9. This very low overlap (~2%) could be explained by the distinct cellular system used (HEK293T and HeLa versus MT4 T cells), the origin of Vpr (Bru versus NL4.3 Vpr), and differences in the configuration of the BirA-Vpr and the approach used to express it.

In this study, we focused our functional analysis on APC/C, and notably its central scaffolding component APC1 (31), as a new HIV-1 Vpr target (Fig. 1 and 2). We provide evidence that Vpr forms a physical complex containing APC1 and APC/C coactivators Cdh1/Cdc20 and mediates the degradation of APC1 (Fig. 4 and 6). As for previously reported Vpr targets (10–14, 16, 18, 32, 45), our results suggest that APC1 degradation relies on the recruitment of a functional DCAF1com by Vpr through DCAF1 and on the presence of an active proteasome (Fig. 5). Taken together, these results support a model in which Vpr would form a complex with APC1 and recruit DCAF1com to induce the polyubiquitination and proteasomal degradation of a central scaffolding component of APC/C, a condition that is likely to impair APC/C activity (31). While a previous AP-MS analysis (11) revealed a potential interaction of Vpr with Cdc20, more studies are warranted to directly assess whether Vpr selectively targets APC/C^{Cdh1} or/and APC/C^{Cdc20} (Fig. 6).

Interestingly, we show that Vpr-mediated APC1 degradation activity is observed with several transmitted/founder primary Vpr variants (Fig. 7), suggesting that the interplay between HIV-1 Vpr and APC/C might be a conserved feature of primary HIV-1 strains. We also found that the Vpr variant derived from the laboratory-adapted virus NL4.3 does not mediate APC1 degradation (Fig. 7), supporting the notion that APC1 depletion and induction of a G_2/M cell cycle arrest are two distinct Vpr activities. Mutagenic analysis of Vpr identified residues N28 and G41 as critical for Vpr-mediated APC1 degradation (Fig. 8). The fact that NL4.3 Vpr is strongly attenuated in its ability to bind APC1 (Fig. 9A and B), despite having only 3 single-amino-acid differences at positions Y15, N28, and G41, points to an important role of these residues in the formation of a complex containing Vpr and APC/C. Importantly, the observation that some HIV-1 Vpr variants display conservation of these residues at these positions underlines further the potential functional importance of Vpr-mediated APC1 degradation. This is not the first report demonstrating that the prototypic NL4.3 virus behaves differently from

primary isolates. For instance, Vpu variants from most HIV-1 primary strains downregulate HLA-C, while the NL4.3 Vpu variant does not (47).

We found that substitution mutations abrogating Vpr-mediated APC1 degradation, namely, N28S and G41N, do not impede viral replication in primary $CD4^+$ T cells or in macrophages (Fig. 10), suggesting that the Vpr-APC1 interplay is not critical for HIV-1 replication, at least in the cellular settings used in this study. However, the conservation of this activity suggests that it might be important for other aspects of HIV-1 pathogenesis. For instance, HIV-1 is heavily uracilated in macrophages, given that reverse transcriptase (RT) fails to distinguish dTTP from UTP during reverse transcription (48, 49). Misincorporation of noncanonical dNTPs into the HIV-1 genome is reported to result in mutations or sensing of the viral genome as "nonself" (48, 50). The fact that key regulators of the dTTP pool, namely, thymidine kinase (TK1) and thymidylate kinase (TMPK), are negatively modulated by APC/C^{Cdh1} and APC/C, respectively (51, 52), raises the interesting possibility that by targeting APC/C, Vpr might increase TK1 and TMPK levels to increase dTTP levels relative to UTP in noncycling macrophages and therefore allow preferential incorporation of dTTP during reverse transcription. Whether Vpr-mediated APC1 degradation impacts the dTTP pool as well as HIV-1 genome uracilation and/or sensing during infection of macrophages warrants further investigations.

Several viral proteins are known to interact with APC/C and consequently modulate APC/C functions during viral infection. For instance, human T cell lymphotropic virus type 1 Tax prematurely activates APC/C^{Cdc20} (53), while the Orf virus PACR (poxvirus anaphase-promoting complex) acts as a competitor of the APC11 subunit (54), and chicken anemia virus apoptin associates with APC/C and displaces it to promyelocytic leukemia (PML) nuclear bodies (39). In most cases, the impact of targeting of APC/C on viral replication remains unclear (30). Interestingly, the interplay between APC/C and its coactivators is regulated by the PP2A phosphatase (55). The adenovirus protein E4orf4 binds the PP2A regulatory B55α subunit and thereby mediates CDK-dependent Cdc20 and Cdh1 phosphorylation, leading to premature APC/C^{Cdc20} activation and inhibition of APC/C^{Cdh1} (56). Given that recent studies have reported that HIV-1 Vif mediates the degradation of the PP2A phosphatase subunit called $PPP2R5^{A-E}$ (57, 58), it will be interesting to determine whether the phosphorylation status of APC/C and its coactivators is affected upon Vif expression. Indeed, some HIV-1 strains might employ multiple accessory proteins and processes to modulate APC/C functions. This redundant concept of modulating APC/C by several accessory proteins might be strong *a priori* evidence of APC/C biological relevance with respect to HIV-1 pathogenesis.

MATERIALS AND METHODS

Cells. HEK293T and HeLa cells were cultured in Dulbecco's modified essential medium (DMEM) (Wisent no. 319-005-CL) supplemented with 10% heat-inactivated fetal bovine serum (FBS; Wisent no. 080-150 or GE HyClone no. SH30396.03). HEK293 Flp-In T-REx (59) and HeLa Flp-In T-REx (from Stephen Taylor [University of Manchester]) (60) were cultured as HEK293T and HeLa cells, except that medium was supplemented with 15 μg/ml blasticidin (InvivoGen no. ANT-BL-1). MT4 $CD4^+$ T cells were cultured in RPMI (Wisent no. 350-000-CL) supplemented with 10% heat-inactivated FBS.

Peripheral blood samples were obtained from HIV- and hepatitis C virus (HCV)-seronegative adults (of either gender). Research protocols for the use of human blood cells were approved by the Research Ethics Review Board of the Montreal Clinical Research Institute (IRCM). All participants had given written informed consent, and all studies were in compliance with the Declaration of Helsinki. MDMs and $CD4^+$ T cells were obtained as previously described (61, 62).

Plasmids. For HA-Vpr plasmids, HIV-1 Vpr were obtained by amplification from source plasmids (WT and mutant [Q65R, S79A, and R80A] Bru) (5); Lai; NL4.3; RHGA (no. 12421), STCOr1 (no. 12417), and WAR0 (no. 12419) were obtained from Beatrice Hahn (University of Pennsylvania) (41) through the NIH AIDS Reagent Program. All Vpr were HA tagged and ligated into a modified pDEST-pcDNA5-BirA-FLAG N-term (63) using HindIII and XhoI restriction sites. Single Bru mutants (H15Y, N28S, and G41N) were obtained from Gene Art Gene Synthesis (Thermo Fisher Scientific) and cloned as indicated above. Vpr double mutants (H15Y-N28S, H15Y-G41N, and N28S-G41N) were generated using site-directed mutagenesis (Q5 site-directed mutagenesis kit; New England Biolabs [NEB] no. E0552S) with the following primer pairs: N28S (F, GGAGCTTAAGAGTGAAGCTGTTAG; R, TCTAAAAGCTCTAGTGTCC; melting temperature [T_m] = 59°C); G41N (F, TTGGCTCCATAACTTAGGGCAAC; R, ATCCTAGGAAAATGTCTAAC; T_m = 57°C).

For the plasmids used in BioID, WT Vpr (Bru variant) and Vpr mutants (Q65R and R80A) were fused at the N terminus with BirA*-Flag by a Gateway cloning strategy in pDEST-pcDNA5-BirA-FLAG N-term using

pDONR-221 (Invitrogen; Thermo Fisher Scientific) as an intermediate. pDEST-pcDNA5-BirA-FLAG N-term and pDEST-pcDNA5-FLAG-NLS-BirA constructs were provided by Anne-Claude Gingras (The Lunenfeld-Tanenbaum Research Institute) (63).

The green fluorescent protein (GFP)-marked WPI lentiviral vectors encoding HA-tagged Vpr proteins were previously described (42). The pOG44 plasmid, encoding the Flp recombinase used to generate the stable cell lines, was obtained from Invitrogen (Thermo Fisher Scientific no. V600520); the Flag-APC1-encoding plasmid was provided by Jose Teodoro (McGill University); the Flag-HLTF-encoding plasmid was provided by Jacek Skowronski (Case Western Reserve University) (11); and both the Myc-Cdh1 (Addgene no. 11595)- and Myc-Cdc20 (Addgene no. 11593)-encoding plasmids were provided by Marc Kirschner (Harvard Medical School) (64).

Stable-cell-line generation, BioID, and liquid chromatography-tandem mass spectrometry (LC-MS/MS). HEK293 Flp-In T-REx and HeLa Flp-In T-REx stably expressing inducible HA-Vpr or BioID constructs (see above) were generated using the Flp-In T-REx system (Thermo Fisher Scientific) (65) and BioID screens were performed as previously described (59, 63). Briefly, two 150-mm plates (around 13×10^6 cells) containing HEK293 Flp-In T-REx or HeLa Flp-In T-REx cells inducibly expressing Flag-NLS-BirA*, BirA*-Flag-VprWT, BirA*-Flag-VprQ65R, or BirA*-Flag-VprR80A were induced with 0.5 μg/ml doxycycline and treated with 50 μM D-biotin (BioBasic no. BB0078) for 6, 7, or 24 h. HEK293-based cell lines induced for 6 h were also treated with a 10 μM concentration of the proteasome inhibitor MG-132 (Calbiochem; MilliporeSigma no. 474787) to prevent proteasomal degradation of potential Vpr targets. After induction, cells were washed once in phosphate-buffered saline (PBS) and lysed for 1 h at 4°C on a wheel in radioimmunoprecipitation assay-deoxycholate (RIPA-DOC) buffer (140 mM NaCl, 8 mM Na_2HPO_4, NaH_2PO_4, 1% NP-40, 0.05% SDS, 5 g/liter sodium deoxycholate, 1× cOmplete mini protease inhibitor cocktail [Roche; MilliporeSigma no. 11836145001]; pH 7.2) supplemented with 200 U Benzonase (EMD Millipore no. 70664) per sample. Samples were then sonicated (450 Sonifier; Branson Ultrasonics Corporation) on ice for 30 s (three cycles of 10 s ON, 5 s OFF) at 20 W. Following sample clarification (5 min, 10,000 × *g*, 4°C), 4 mg of proteins was mixed with 200 μl of prewashed streptavidin Sepharose high-performance beads (GE Healthcare no. 17-5113-01) and incubated on a wheel for 3 to 4 h. Beads were washed once in RIPA-DOC buffer and four additional times in 50 mM ammonium bicarbonate (pH 8.5).

The on-bead proteins were digested and harvested as previously described (59). Peptides were then reduced and alkylated, and detergent residue was removed by MCX (96-well Oasis MCX μElution plate; Waters no. 186001830BA) following the manufacturer's instructions. After elution in 10% ammonium hydroxide/90% methanol (vol/vol), samples were dried, reconstituted in 5% formic acid, and injected on an LTQ Orbitrap Velos equipped with a Proxeon nanoelectrospray Flex ion (Thermo Fisher Scientific) source as previously described (59).

Mass spectrometry data analyses. Raw mass spectrometry files were analyzed with the search engines Mascot, X!Tandem, and Comet through the iProphet pipeline integrated in Prohits (66), using the UniProt database (v20160623) supplemented with "common contaminants" from the Max Planck Institute (http://maxquant.org), the Global Proteome Machine (GPM; http://www.thegpm.org/crap/index.html), and decoy sequences. The parameters were set with trypsin specificity (two missed cleavage sites allowed); variable modifications involved oxidation (M), deamidation (NQ), biotin (K), biotin (N-Term), and ubiquitin (K), and fixed modification was set with carbamidomethyl (C). The mass tolerance for precursor and fragment ions was set to 15 ppm and 0.6 Da, respectively, and peptide charges of +2, +3, and +4 were considered. The resulting search results were individually processed by PeptideProphet, and peptides were assembled into proteins using parsimony rules first described in ProteinProphet using the Trans-Proteomic Pipeline (TPP) with the following settings: -p 0.05 -x20 -PPM "DECOY"; iProphet options: pPRIME and PeptideProphet: pP.

Interaction scoring. To estimate interaction statistics, we used SAINTexpress (v3.6.1) on proteins with an iProphet protein probability of ≥0.9 and a unique-peptides value of ≥2 (67). Each of the proteomics data sets (HEK293 [6 or 24 h] and HeLa [24 h]) was compared separately against its respective negative control (Flag-NLS-BirA* or WT Vpr from MG132-untreated HEK293 cells). SAINT analyses were performed with the following settings: nControl:2, nCompressBaits:2 (no baits compression). Interactions displaying a BFDR of ≤0.02 were considered statistically significant and kept. Unfiltered contaminants, such as keratins, BirA*, beta-galactosidase, ribosomal subunits, and carboxylases, were considered contaminants and removed.

Bioinformatics analyses. Proteomic data and annotation databases, such as BioGRID (human v3.4.164), UniProt (human; released on October 2017) and the Gene Ontology (GO) annotation database, were imported into a local MySQL database (68). Graphical representations of protein-protein networks were generated with Cytoscape (v3.7.0). Network augmentations of our BioID screens were performed by extracting prey-prey interactions from the human BioGRID network and from Cytoscape's PSICQUIC Web Service client (released in October 2018) searching the IntAct, iRefIndex, Reactome, and UniProt databases. Individual networks from the HEK293 (6 and 24 h) and HeLa (24 h) cells were merged together into one Vpr proximity interaction network and clustered using GO enrichment analysis and PANTHER classification system (http://geneontology.org/). Interactions were clustered, and the following functions were extracted based on the GO associated with each node within the network: response to DNA damage, cell cycle, RNA processing, and gene expression. Heat maps were generated with the Pheatmap package (without clustering) in R (www.r-project.org) with average spectral counts rescaled from 0 to 1 for each protein among the 3 samples (WT−MG132, Q65R+MG132, and WT+MG132) with the R scales package. Protein complexes were identified with the CORUM database (69).

Transfection and cycloheximide treatment. HEK293T were transfected with the indicated plasmids using the calcium phosphate precipitation method. At 42 h posttransfection, cells were treated with 20 μg/ml cycloheximide (Calbiochem; MilliporeSigma no. 239764) to inhibit translation, allowing analysis

of a preset pool of proteins. At 6 h posttreatment, cells were harvested and processed for immunoblotting by Western blotting.

SDS-PAGE and Western blot analysis. Cells were lysed in RIPA-DOC buffer for ≥30 min at 4°C. Lysates were then clarified by centrifugation (5 min, 10,000 × *g*, 4°C), and protein amounts were quantified by Bradford assay (Bio-Rad no. 5000006) and analyzed by Western blotting as previously described (5). The following primary antibodies were used: anti-HA (BioLegend no. 901513), anti-Flag (MilliporeSigma no. F3165), anti-Myc (MilliporeSigma no. C3956), anti-APC1 (Abcam no ab133397), anti-HLTF (Bethyl no. A300-230A), anti-DCAF1 (Bethyl no. A301-887A), anti-GFP (MilliporeSigma no. SAB4301138), anti-actin (MP Biomedicals no. 0869100), anti-GAPDH (BioLegend no. 649202), and anti-lamin B1 (Abcam no. ab16048). Horseradish peroxidase (HRP)-conjugated secondary antibodies were from Bio-Rad (no. 170-6515 and no. 170-6516). Quantification of bands was performed using Image J (v1.52).

siRNA-mediated protein knockdown. DCAF1 knockdown in HEK293T was performed with Lipofectamine RNAiMAX (Thermo Fisher Scientific no. 13778150) according to the manufacturer's instructions and as previously described (5). The following siRNAs were used: DCAF1 (Dharmacon no. M-021119-01) and scrambled (Dharmacon no. D-001210-02). After siRNA transfection, cells were subjected to transfection of plasmids of interest using the above-mentioned protocol.

Coimmunoprecipitation. At 48 h posttransfection, HEK293T cells were washed once in DMEM, harvested, and lysed in ice-cold Triton lysis buffer (150 mM NaCl, 50 mM Tris, 0.5% Triton X-100, 1× cOmplete mini-protease inhibitors without EDTA [Roche-MilliporeSigma no. 11873580001]; pH 7.25) for 30 min and clarified (5 min, 10,000 × *g*, 4°C). For HA coimmunoprecipitation (co-IP), 1.5 mg of proteins was mixed with 50 μl anti-HA agarose beads (MilliporeSigma no. A-2095) and incubated at 4°C for 3 h on a wheel. For Myc co-IP, 1.5 mg of proteins was mixed with 2.5 μg anti-Myc antibody (MilliporeSigma no. C3956) and incubated at 4°C, and after 2 h, 100 μl protein A-Sepharose beads (Invitrogen; Thermo Fisher Scientific no. 101041) was added to the mixture. Following incubation for 1 h at 4°C, beads were washed three times in lysis buffer, resuspended in Laemmli buffer, boiled for 5 min, and loaded on SDS-PAGE gels for Western blotting.

Cell cycle analysis. Cell cycle analyses of transfected HEK293T or of infected MT4 were performed by flow cytometry (BD FACSCalibur; Becton Dickinson) as previously described (45). The ModFit mathematical model (v4.1.7; Verity Software House) was used to determine the proportion of cells in G_1 and G_2/M phases, and the ratio of G_2/M to G_1 was calculated.

Confocal microscopy. APC1 and HA-Vpr localization was determined by confocal microscopy as previously described (70). HA-Vpr-inducible HeLa cells were treated with 0.5 μg/ml doxycycline for 16 to 18 h. Alternatively, HeLa cells were transfected with Vpr-expressing plasmids using Lipofectamine 2000 (Invitrogen; Thermo Fisher Scientific no. 11668019) for 24 h. Cells were then fixed, permeabilized, and incubated with anti-HA (1/500; BioLegend no. 901513) and anti-APC1 (1/250; Abcam no. ab133397) for 1 h at 37°C. The following secondary antibodies were used for 30 min at 37°C: Alexa Fluor 488-conjugated anti-mouse IgG (1/500; Invitrogen; Thermo Fisher Scientific no. A-11001) and Alexa Fluor 647-conjugated anti-rabbit IgG (1/500; Invitrogen; Thermo Fisher Scientific no. A-21244). Pictures were acquired using 43× or 63× oil immersion objectives on an inverted LSM710 confocal microscope (Zeiss). APC1 and HA-Vpr colocalization was determined using ImageJ (v1.52).

Vpr sequence alignments. Primary amino acid sequences from Bru and NL4.3 Vpr variants were aligned using Clustal Omega from the European Bioinformatics Institute (v1.2.4; EMBL-EBI; https://www.ebi.ac.uk/Tools/msa/clustalo/). The percentage of conservation of Vpr residues at positions 28 and 41 was determined using nucleotide sequences from 4 835 HIV-1 strains obtained from the HIV Sequence Database (Los Alamos National Laboratory; http://www.hiv.lanl.gov/), translated, and aligned with Jalview (v2.11.0).

Proviral constructs, virus production, and infection. The isogenic proviruses HxBru-ADA-GFP encoding WT Vpr or defective for Vpr (dVpr) were described previously (42). HxBru-ADA-GFP harboring the N28S-G41N Vpr double substitution was generated by SDM and validated by sequencing. Infectious VSV-G-pseudotyped HIV-1 viruses were produced by transfection of proviral constructs with a plasmid encoding VSV-G in HEK293T by the calcium phosphate transfection method (42). After 48 h, culture supernatant was harvested and ultracentrifuged onto a 20% sucrose cushion to concentrate viruses. Viral titers were determined by analyzing the percentage of GFP^+ cells in infected HeLa cells by flow cytometry at 24 h postinfection.

MT4 cells were infected at a multiplicity of infection (MOI) of 0.75 and processed for cell cycle analysis 24 h later. MDMs were infected at an MOI of 1, and the percent infection was determined by measurement of GFP by flow cytometry (SA3800 spectral analyzer; Sony Biotechnology) every 3 days (61). Primary $CD4^+$ T cells were infected at MOI of 0.1 and 0.5, and the percent GFP-positive cells was monitored daily by flow cytometry (62).

Immunostaining and flow cytometry. MDMs were infected as described above. After 3 days, cells were harvested, fixed with 4% formaldehyde, permeabilized with 0.2% Triton X-100, and blocked as previously described (61). Vpr was detected by immunostaining using an anti-Vpr monoclonal primary antibody (1/200; clone 8D1; obtained from Yukihito Ishizaka [National Center for Global Health and Medicine, Tokyo, Japan] [71]; commercially available as Cosmo Bio no. CAC-NCG-M01-1) and a secondary Alexa Fluor 647-conjugated anti-mouse antibody (1/100; Invitrogen; Thermo Fisher Scientific no. A-21236). Vpr levels in the GFP^+ population were determined by flow cytometry (BD LSRFortessa; Becton Dickinson) and analyzed using FlowJo (v9.3.2).

Statistics. Statistical analyses were done using GraphPad Prism 5.03 or 8.2.1. *P* values of less than 0.05 were considered statistically significant. Statistically significant differences (*P* values of ≤0.05, ≤0.01, and ≤0.001) relative to the no-Vpr control were determined by two-tailed paired Student's *t* tests or as indicated.

SUPPLEMENTAL MATERIAL

Supplemental material is available online only.

SUPPLEMENTAL FILE 1, XLSX file, 1.3 MB.

SUPPLEMENTAL FILE 2, XLSX file, 0.05 MB.

SUPPLEMENTAL FILE 3, XLSX file, 0.4 MB.

ACKNOWLEDGMENTS

We thank the Mass Spectrometry and Proteomics, the Flow Cytometry, the Microscopy, and the Molecular Biology core facilities of the Montreal Clinical Research Institute (IRCM) for their support and assistance. We are also grateful to Jean-François Côté, Halil Bagci, and Christian Poitras for their assistance and helpful discussions regarding the BioID experiments. We thank Martine Gauthier from the IRCM Clinic for coordinating access to blood donors, as well as the blood donor participants. The following reagents were obtained from the NIH AIDS Reagent Program, Division of AIDS, NIAID, NIH: RHGA (no. 12421), STCOr1 (no. 12417), and WAR0 (no. 12419), obtained from Beatrice Hahn. We also thank Jean-François Côté, Anne-Claude Gingras, Yukihito Ishizaka, Marc Kirschner, Jacek Skowronski, Stephen Taylor, and Jose Teodoro for providing reagents as well as Tram N. Q. Pham for her critical review of the manuscript.

This study was supported by a Canadian Institutes of Health Research (CIHR) Foundation grant (HB2-164064) to É.A.C. É.A.C. is a recipient of the IRCM-Université de Montréal Chair of Excellence in HIV research. J.A.F.B. was awarded doctoral scholarships from the IRCM Foundation and Université de Montréal.

REFERENCES

1. Malim MH, Emerman M. 2008. HIV-1 accessory proteins: ensuring viral survival in a hostile environment. Cell Host Microbe 3:388–398. https://doi.org/10.1016/j.chom.2008.04.008.
2. Romani B, Cohen EA. 2012. Lentivirus Vpr and Vpx accessory proteins usurp the cullin4-DDB1 (DCAF1) E3 ubiquitin ligase. Curr Opin Virol 2:755–763. https://doi.org/10.1016/j.coviro.2012.09.010.
3. Roshal M, Kim B, Zhu Y, Nghiem P, Planelles V. 2003. Activation of the ATR-mediated DNA damage response by the HIV-1 viral protein R. J Biol Chem 278:25879–25886. https://doi.org/10.1074/jbc.M303948200.
4. Planelles V, Jowett JBM, Li QX, Xie Y, Hahn B, Chen IS. 1996. Vpr-induced cell cycle arrest is conserved among primate lentiviruses. J Virol 70:2516–2524. https://doi.org/10.1128/JVI.70.4.2516-2524.1996.
5. Belzile JP, Duisit G, Rougeau N, Mercier J, Finzi A, Cohen EA. 2007. HIV-1 Vpr-mediated G2 arrest involves the DDB1-CUL4A-VPRBP E3 ubiquitin ligase. PLoS Pathog 3:e85. https://doi.org/10.1371/journal.ppat.0030085.
6. Le Rouzic E, Belaidouni N, Estrabaud E, Morel M, Rain JC, Transy C, Margottin-Goguet F. 2007. HIV1 Vpr arrests the cell cycle by recruiting DCAF1/VprBP, a receptor of the Cul4-DDB1 ubiquitin ligase. Cell Cycle 6:182–188. https://doi.org/10.4161/cc.6.2.3732.
7. Hrecka K, Gierszewska M, Srivastava S, Kozaczkiewicz L, Swanson SK, Florens L, Washburn MP, Skowronski J. 2007. Lentiviral Vpr usurps Cul4-DDB1[VprBP] E3 ubiquitin ligase to modulate cell cycle. Proc Natl Acad Sci U S A 104:11778–11783. https://doi.org/10.1073/pnas.0702102104.
8. DeHart JL, Zimmerman ES, Ardon O, Monteiro-Filho CM, Arganaraz ER, Planelles V. 2007. HIV-1 Vpr activates the G2 checkpoint through manipulation of the ubiquitin proteasome system. Virol J 4:57. https://doi.org/10.1186/1743-422X-4-57.
9. Schrofelbauer B, Hakata Y, Landau NR. 2007. HIV-1 Vpr function is mediated by interaction with the damage-specific DNA-binding protein DDB1. Proc Natl Acad Sci U S A 104:4130–4135. https://doi.org/10.1073/pnas.0610167104.
10. Belzile JP, Richard J, Rougeau N, Xiao Y, Cohen EA. 2010. HIV-1 Vpr induces the K48-linked polyubiquitination and proteasomal degradation of target cellular proteins to activate ATR and promote G2 arrest. J Virol 84:3320–3330. https://doi.org/10.1128/JVI.02590-09.
11. Hrecka K, Hao C, Shun MC, Kaur S, Swanson SK, Florens L, Washburn MP, Skowronski J. 2016. HIV-1 and HIV-2 exhibit divergent interactions with HLTF and UNG2 DNA repair proteins. Proc Natl Acad Sci U S A 113:E3921–E3230. https://doi.org/10.1073/pnas.1605023113.
12. Lahouassa H, Blondot ML, Chauveau L, Chougui G, Morel M, Leduc M, Guillonneau F, Ramirez BC, Schwartz O, Margottin-Goguet F. 2016. HIV-1 Vpr degrades the HLTF DNA translocase in T cells and macrophages. Proc Natl Acad Sci U S A 113:5311–5316. https://doi.org/10.1073/pnas.1600485113.
13. Yan J, Shun MC, Hao C, Zhang Y, Qian J, Hrecka K, DeLucia M, Monnie C, Ahn J, Skowronski J. 2018. HIV-1 Vpr reprograms CLR4(DCAF1) E3 ubiquitin ligase to antagonize exonuclease 1-mediated restriction of HIV-1 infection. mBio 9:e01732-18. https://doi.org/10.1128/mBio.01732-18.
14. Laguette N, Bregnard C, Hue P, Basbous J, Yatim A, Larroque M, Kirchhoff F, Constantinou A, Sobhian B, Benkirane M. 2014. Premature activation of the SLX4 complex by Vpr promotes G2/M arrest and escape from innate immune sensing. Cell 156:134–145. https://doi.org/10.1016/j.cell.2013.12.011.
15. Fregoso OI, Emerman M. 2016. Activation of the DNA damage response is a conserved function of HIV-1 and HIV-2 Vpr that is independent of SLX4 recruitment. mBio 7:e01433-16. https://doi.org/10.1128/mBio.01433-16.
16. Schrofelbauer B, Yu Q, Zeitlin SG, Landau NR. 2005. Human immunodeficiency virus type 1 Vpr induces the degradation of the UNG and SMUG uracil-DNA glycosylases. J Virol 79:10978–10987. https://doi.org/10.1128/JVI.79.17.10978-10987.2005.
17. Connor RI, Chen BK, Choe S, Landau NR. 1995. Vpr is required for efficient replication of human immunodeficiency virus type-1 in mononuclear phagocytes. Virology 206:935–944. https://doi.org/10.1006/viro.1995.1016.
18. Lv L, Wang Q, Xu Y, Tsao LC, Nakagawa T, Guo H, Su L, Xiong Y. 2018. Vpr targets TET2 for degradation by CRL4(VprBP) E3 ligase to sustain IL-6 expression and enhance HIV-1 replication. Mol Cell 70:961–970.E5. https://doi.org/10.1016/j.molcel.2018.05.007.
19. Wang Q, Su L. 2019. Vpr enhances HIV-1 Env processing and virion infectivity in macrophages by modulating TET2-dependent IFITM3 expression. mBio 10:e01344-19. https://doi.org/10.1128/mBio.01344-19.
20. Lubow J, Virgilio MC, Merlino M, Collins DR, Mashiba M, Peterson BG, Lukic Z, Painter MM, Gomez-Rivera F, Terry V, Zimmerman G, Collins KL. 2020. Mannose receptor is an HIV restriction factor counteracted by Vpr in macrophages. Elife 9:e51035. https://doi.org/10.7554/eLife.51035.
21. Gibbons JM, Marno KM, Pike R, Lee WJ, Jones CE, Ogunkolade BW, Pardieu C, Bryan A, Fu RM, Warnes G, Rowley PA, Sloan RD, McKnight A. 2019. HIV-1 accessory protein Vpr interacts with REAF/RPRD2 to mitigate its antiviral activity. J Virol 94:e01591-19. https://doi.org/10.1128/JVI.01591-19.
22. Jäger S, Cimermancic P, Gulbahce N, Johnson JR, McGovern KE, Clarke SC, Shales M, Mercenne G, Pache L, Li K, Hernandez H, Jang GM, Roth SL, Akiva E, Marlett J, Stephens M, D'Orso I, Fernandes J, Fahey M, Mahon C, O'Donoghue AJ, Todorovic A, Morris JH, Maltby DA, Alber T, Cagney G, Bushman FD, Young JA, Chanda SK, Sundquist WI, Kortemme T, Hernandez RD, Craik CS, Burlingame A, Sali A, Frankel AD, Krogan NJ. 2011. Global landscape of HIV-

human protein complexes. Nature 481:365–370. https://doi.org/10.1038/nature10719.
23. Greenwood EJD, Williamson JC, Sienkiewicz A, Naamati A, Matheson NJ, Lehner PJ. 2019. Promiscuous targeting of cellular proteins by Vpr drives systems-level proteomic remodeling in HIV-1 infection. Cell Rep 27:1579–1596.E7. https://doi.org/10.1016/j.celrep.2019.04.025.
24. Yan J, Shun MC, Zhang Y, Hao C, Skowronski J. 2019. HIV-1 Vpr counteracts HLTF-mediated restriction of HIV-1 infection in T cells. Proc Natl Acad Sci U S A 116:9568–9577. https://doi.org/10.1073/pnas.1818401116.
25. Roux KJ, Kim DI, Raida M, Burke B. 2012. A promiscuous biotin ligase fusion protein identifies proximal and interacting proteins in mammalian cells. J Cell Biol 196:801–810. https://doi.org/10.1083/jcb.201112098.
26. Peters JM. 2006. The anaphase promoting complex/cyclosome: a machine designed to destroy. Nat Rev Mol Cell Biol 7:644–656. https://doi.org/10.1038/nrm1988.
27. Prinz S, Hwang ES, Visintin R, Amon A. 1998. The regulation of CDC20 proteolysis reveals a role for APC components CDC23 and CDC27 during S phase and early mitosis. Curr Biol 8:750–760. https://doi.org/10.1016/S0960-9822(98)70298-2.
28. Jaspersen SL, Charles JF, Morgan DO. 1999. Inhibitory phosphorylation of the APC regulator HCT1 is controlled by the kinase CDC28 and the phosphatase CDC14. Curr Biol 9:227–236. https://doi.org/10.1016/s0960-9822(99)80111-0.
29. Zhou Z, He M, Shah AA, Wan Y. 2016. Insights into APC/C: from cellular function to diseases and therapeutics. Cell Div 11:9. https://doi.org/10.1186/s13008-016-0021-6.
30. Mo M, Shahar S, Fleming SB, Mercer AA. 2012. How viruses affect the cell cycle through manipulation of the APC/C. Trends Microbiol 20:440–448. https://doi.org/10.1016/j.tim.2012.05.007.
31. Thornton BR, Ng TM, Matyskiela ME, Carroll CW, Morgan DO, Toczyski DP. 2006. An architectural map of the anaphase-promoting complex. Genes Dev 20:449–460. https://doi.org/10.1101/gad.1396906.
32. Klockow LC, Sharifi HJ, Wen X, Flagg M, Furuya AK, Nekorchuk M, de Noronha CM. 2013. The HIV-1 protein Vpr targets the endoribonuclease Dicer for proteasomal degradation to boost macrophage infection. Virology 444:191–202. https://doi.org/10.1016/j.virol.2013.06.010.
33. Micklem G, Rowley A, Harwood J, Nasmyth K, Diffley JF. 1993. Yeast origin recognition complex is involved in DNA replication and transcriptional silencing. Nature 366:87–89. https://doi.org/10.1038/366087a0.
34. Treiber T, Treiber N, Meister G. 2019. Regulation of microRNA biogenesis and its crosstalk with other cellular pathways. Nat Rev Mol Cell Biol 20:5–20. https://doi.org/10.1038/s41580-019-0106-6.
35. Inada T, Makino S. 2014. Novel roles of the multi-functional CCR4-NOT complex in post-transcriptional regulation. Front Genet 5:135. https://doi.org/10.3389/fgene.2014.00135.
36. Battle DJ, Kasim M, Yong J, Lotti F, Lau CK, Mouaikel J, Zhang Z, Han K, Wan L, Dreyfuss G. 2006. The SMN complex: an assembly machine for RNPs. Cold Spring Harbor Symp Quant Biol 71:313–320. https://doi.org/10.1101/sqb.2006.71.001.
37. Wang Y, Cortez D, Yazdi P, Neff N, Elledge SJ, Qin J. 2000. BASC, a super complex of BRCA1-associated proteins involved in the recognition and repair of aberrant DNA structures. Genes Dev 14:927–939.
38. Greil C, Krohs J, Schnerch D, Follo M, Felthaus J, Engelhardt M, Wasch R. 2016. The role of APC/C(Cdh1) in replication stress and origin of genomic instability. Oncogene 35:3062–3070. https://doi.org/10.1038/onc.2015.367.
39. Teodoro JG, Heilman DW, Parker AE, Green MR. 2004. The viral protein apoptin associates with the anaphase-promoting complex to induce G2/M arrest and apoptosis in the absence of p53. Genes Dev 18:1952–1957. https://doi.org/10.1101/gad.1198404.
40. Clark AE, Spector DH. 2015. Studies on the contribution of human cytomegalovirus UL21a and UL97 to viral growth and inactivation of the anaphase-promoting complex/cyclosome (APC/C) E3 ubiquitin ligase reveal a unique cellular mechanism for downmodulation of the APC/C subunits APC1, APC4, and APC5. J Virol 89:6928–6939. https://doi.org/10.1128/JVI.00403-15.
41. Parrish NF, Gao F, Li H, Giorgi EE, Barbian HJ, Parrish EH, Zajic L, Iyer SS, Decker JM, Kumar A, Hora B, Berg A, Cai F, Hopper J, Denny TN, Ding H, Ochsenbauer C, Kappes JC, Galimidi RP, West AP, Jr, Bjorkman PJ, Wilen CB, Doms RW, O'Brien M, Bhardwaj N, Borrow P, Haynes BF, Muldoon M, Theiler JP, Korber B, Shaw GM, Hahn BH. 2013. Phenotypic properties of transmitted founder HIV-1. Proc Natl Acad Sci U S A 110:6626–6633. https://doi.org/10.1073/pnas.1304288110.
42. Richard J, Sindhu S, Pham TN, Belzile JP, Cohen EA. 2010. HIV-1 Vpr up-regulates expression of ligands for the activating NKG2D receptor and promotes NK cell-mediated killing. Blood 115:1354–1363. https://doi.org/10.1182/blood-2009-08-237370.
43. Balliet JW, Kolson DL, Eiger G, Kim FM, McGann KA, Srinivasan A, Collman R. 1994. Distinct effects in primary macrophages and lymphocytes of the human immunodeficiency virus type 1 accessory genes Vpr, Vpu, and Nef: mutational analysis of a primary HIV-1 isolate. Virology 200:623–631. https://doi.org/10.1006/viro.1994.1225.
44. Forouzanfar F, Ali S, Wallet C, De Rovere M, Ducloy C, El Mekdad H, El Maassarani M, Ait-Ammar A, Van Assche J, Boutant E, Daouad F, Margottin-Goguet F, Moog C, Van Lint C, Schwartz C, Rohr O. 2019. HIV-1 Vpr mediates the depletion of the cellular repressor CTIP2 to counteract viral gene silencing. Sci Rep 9:13154. https://doi.org/10.1038/s41598-019-48689-x.
45. Hossain D, Ferreira Barbosa JA, Cohen EA, Tsang WY. 2018. HIV-1 Vpr hijacks EDD-DYRK2-DDB1(DCAF1) to disrupt centrosome homeostasis. J Biol Chem 293:9448–9460. https://doi.org/10.1074/jbc.RA117.001444.
46. Zhang F, Bieniasz PD. 2020. HIV-1 Vpr induces cell cycle arrest and enhances viral gene expression by depleting CCDC137. Elife 9:e55806. https://doi.org/10.7554/eLife.55806.
47. Apps R, Del Prete GQ, Chatterjee P, Lara A, Brumme ZL, Brockman MA, Neil S, Pickering S, Schneider DK, Piechocka-Trocha A, Walker BD, Thomas R, Shaw GM, Hahn BH, Keele BF, Lifson JD, Carrington M. 2016. HIV-1 Vpu mediates HLA-C downregulation. Cell Host Microbe 19:686–695. https://doi.org/10.1016/j.chom.2016.04.005.
48. Hansen EC, Ransom M, Hesselberth JR, Hosmane NN, Capoferri AA, Bruner KM, Pollack RA, Zhang H, Drummond MB, Siliciano JM, Siliciano R, Stivers JT. 2016. Diverse fates of uracilated HIV-1 DNA during infection of myeloid lineage cells. Elife 5:e18447. https://doi.org/10.7554/eLife.18447.
49. Kennedy EM, Daddacha W, Slater R, Gavegnano C, Fromentin E, Schinazi RF, Kim B. 2011. Abundant non-canonical dUTP found in primary human macrophages drives its frequent incorporation by HIV-1 reverse transcriptase. J Biol Chem 286:25047–25055. https://doi.org/10.1074/jbc.M111.234047.
50. Sire J, Querat G, Esnault C, Priet S. 2008. Uracil within DNA: an actor of antiviral immunity. Retrovirology 5:45. https://doi.org/10.1186/1742-4690-5-45.
51. Ke PY, Chang ZF. 2004. Mitotic degradation of human thymidine kinase 1 is dependent on the anaphase-promoting complex/cyclosome-CDH1-mediated pathway. Mol Cell Biol 24:514–526. https://doi.org/10.1128/mcb.24.2.514-526.2004.
52. Ke PY, Kuo YY, Hu CM, Chang ZF. 2005. Control of dTTP pool size by anaphase promoting complex/cyclosome is essential for the maintenance of genetic stability. Genes Dev 19:1920–1933. https://doi.org/10.1101/gad.1322905.
53. Liu B, Hong S, Tang Z, Yu H, Giam CZ. 2005. HTLV-I Tax directly binds the CDC20-associated anaphase-promoting complex and activates it ahead of schedule. Proc Natl Acad Sci U S A 102:63–68. https://doi.org/10.1073/pnas.0406424101.
54. Mo M, Fleming SB, Mercer AA. 2009. Cell cycle deregulation by a poxvirus partial mimic of anaphase-promoting complex subunit 11. Proc Natl Acad Sci U S A 106:19527–19532. https://doi.org/10.1073/pnas.0905893106.
55. Fujimitsu K, Yamano H. 2020. PP2A-B56 binds to APC1 and promotes CDC20 association with the APC/C ubiquitin ligase in mitosis. EMBO Rep 21:e48503. https://doi.org/10.15252/embr.201948503.
56. Mui MZ, Roopchand DE, Gentry MS, Hallberg RL, Vogel J, Branton PE. 2010. Adenovirus protein E4ORF4 induces premature APC-CDC20 activation in Saccharomyces cerevisiae by a protein phosphatase 2A-dependent mechanism. J Virol 84:4798–4809. https://doi.org/10.1128/JVI.02434-09.
57. Greenwood EJ, Matheson NJ, Wals K, van den Boomen DJ, Antrobus R, Williamson JC, Lehner PJ. 2016. Temporal proteomic analysis of HIV infection reveals remodelling of the host phosphoproteome by lentiviral Vif variants. Elife 5:e18296. https://doi.org/10.7554/eLife.18296.
58. Salamango DJ, Ikeda T, Moghadasi SA, Wang J, McCann JL, Serebrenik AA, Ebrahimi D, Jarvis MC, Brown WL, Harris RS. 2019. HIV-1 Vif triggers cell cycle arrest by degrading cellular PPP2R5 phospho-regulators. Cell Rep 29:1057–1065.E4. https://doi.org/10.1016/j.celrep.2019.09.057.
59. Bagci H, Sriskandarajah N, Robert A, Boulais J, Elkholi IE, Tran V, Lin ZY, Thibault MP, Dube N, Faubert D, Hipfner DR, Gingras AC, Côté JF. 2020. Mapping the proximity interaction network of the Rho-family GTPases reveals signalling pathways and regulatory mechanisms. Nat Cell Biol 22:120–134. https://doi.org/10.1038/s41556-019-0438-7.

60. Tighe A, Staples O, Taylor S. 2008. MPS1 kinase activity restrains anaphase during an unperturbed mitosis and targets MAD2 to kinetochores. J Cell Biol 181:893–901. https://doi.org/10.1083/jcb.200712028.
61. Lodge R, Ferreira Barbosa JA, Lombard-Vadnais F, Gilmore JC, Deshiere A, Gosselin A, Wiche Salinas TR, Bego MG, Power C, Routy JP, Ancuta P, Tremblay MJ, Cohen EA. 2017. Host microRNAs-221 and -222 inhibit HIV-1 entry in macrophages by targeting the CD4 viral receptor. Cell Rep 21:141–153. https://doi.org/10.1016/j.celrep.2017.09.030.
62. Bego MG, Cong L, Mack K, Kirchhoff F, Cohen EA. 2016. Differential control of BST2 restriction and plasmacytoid dendritic cell antiviral response by antagonists encoded by HIV-1 group M and O strains. J Virol 90:10236–10246. https://doi.org/10.1128/JVI.01131-16.
63. Lambert JP, Tucholska M, Go C, Knight JD, Gingras AC. 2015. Proximity biotinylation and affinity purification are complementary approaches for the interactome mapping of chromatin-associated protein complexes. J Proteomics 118:81–94. https://doi.org/10.1016/j.jprot.2014.09.011.
64. Pfleger CM, Lee E, Kirschner MW. 2001. Substrate recognition by the CDC20 and CDH1 components of the anaphase-promoting complex. Genes Dev 15:2396–2407. https://doi.org/10.1101/gad.918201.
65. O'Gorman S, Fox DT, Wahl GM. 1991. Recombinase-mediated gene activation and site-specific integration in mammalian cells. Science 251:1351–1355. https://doi.org/10.1126/science.1900642.
66. Liu G, Zhang J, Larsen B, Stark C, Breitkreutz A, Lin ZY, Breitkreutz BJ, Ding Y, Colwill K, Pasculescu A, Pawson T, Wrana JL, Nesvizhskii AI, Raught B, Tyers M, Gingras AC. 2010. ProHits: integrated software for mass spectrometry-based interaction proteomics. Nat Biotechnol 28:1015–1017. https://doi.org/10.1038/nbt1010-1015.
67. Teo G, Liu G, Zhang J, Nesvizhskii AI, Gingras AC, Choi H. 2014. SAINTexpress: improvements and additional features in Significance Analysis of INTeractome software. J Proteomics 100:37–43. https://doi.org/10.1016/j.jprot.2013.10.023.
68. Chatr-Aryamontri A, Oughtred R, Boucher L, Rust J, Chang C, Kolas NK, O'Donnell L, Oster S, Theesfeld C, Sellam A, Stark C, Breitkreutz BJ, Dolinski K, Tyers M. 2017. The BioGRID interaction database: 2017 update. Nucleic Acids Res 45:D369–D379. https://doi.org/10.1093/nar/gkw1102.
69. Giurgiu M, Reinhard J, Brauner B, Dunger-Kaltenbach I, Fobo G, Frishman G, Montrone C, Ruepp A. 2019. CORUM: the comprehensive resource of mammalian protein complexes-2019. Nucleic Acids Res 47:D559–D563. https://doi.org/10.1093/nar/gky973.
70. Belzile JP, Abrahamyan LG, Gerard FC, Rougeau N, Cohen EA. 2010. Formation of mobile chromatin-associated nuclear foci containing HIV-1 Vpr and VPRBP is critical for the induction of G2 cell cycle arrest. PLoS Pathog 6:e1001080. https://doi.org/10.1371/journal.ppat.1001080.
71. Hoshino S, Sun B, Konishi M, Shimura M, Segawa T, Hagiwara Y, Koyanagi Y, Iwamoto A, Mimaya J, Terunuma H, Kano S, Ishizaka Y. 2007. Vpr in plasma of HIV type 1-positive patients is correlated with the HIV type 1 RNA titers. AIDS Res Hum Retroviruses 23:391–397. https://doi.org/10.1089/aid.2006.0124.